Glacier National Park Progress Report
March 2014
Prepared by Tim Assal and Jason Sibold
Colorado State University

Our initial objective was to investigate the influence of the 1970s mountain pine beetle (MPB) outbreak on subsequent wildfire severity. We planned to use the US Forest Service annual forest health aerial detection surveys (ADS). However, within Glacier National Park the historical ADS data rarely included information on the number of trees killed per acre (severity), which is commonly included in contemporary ADS data and is critical to relating outbreaks to forest processes and change. Furthermore, the forest patches identified in the ADS data were very large (e.g. > 70,000 ha) and even incorporated areas that did not have host species for mountain pine beetle. Although useful for broad-scale monitoring, we suspect the historical ADS data does not represent the heterogeneous impacts of the disturbance. Because both MPB outbreaks and wildfires are heterogeneous at relatively fine scales (~20-30m), identifying relationships between the two disturbances necessitated a more fine-scale map of the MPB outbreak. Consequently, developing a method that used archival remote sensing data to reconstruct the MPB outbreak became the primary focus of this project.

In the first phase of our work, we developed a new method for reconstructing past bark beetle outbreaks using a novel combination of multiple lines of evidence, including aerial photography and Landsat imagery (Figure 1). The lack of spatially explicit data on this disturbance represents both a major data gap and a critical research challenge in that wildfire fire has removed some of the evidence from the landscape. This is a critical first step in our overall goal of identifying the ecological consequences of the interactions of bark beetles with subsequent fire events over the last several decades in the US Rocky Mountains. We believe the method provides a quantitative application of remote sensing to forest disturbance. Furthermore, our work affords a

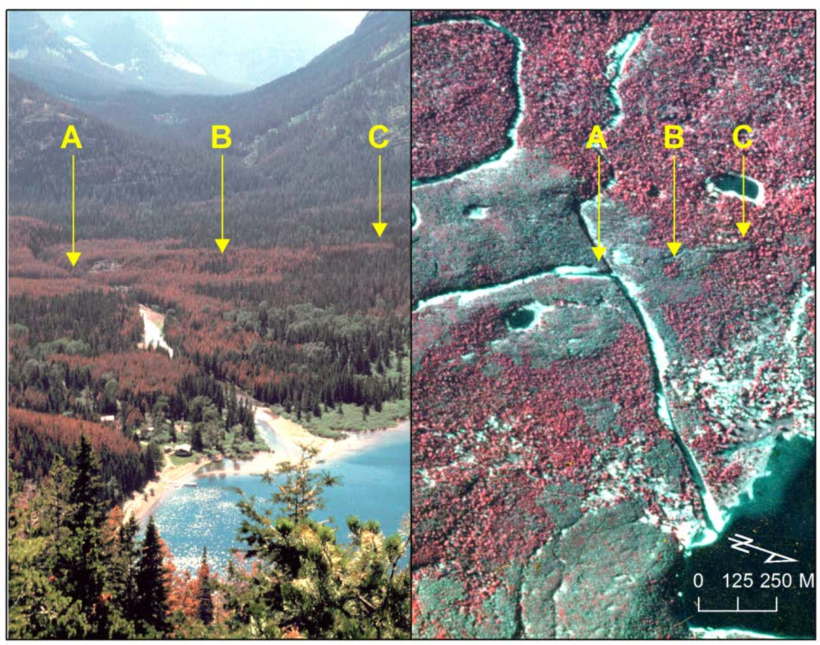

Figure 1. (Left) Landscape photo taken in the Summer of 1980 showing a mixture of live and dead trees in the red attack stage in Waterton Valley (source: Glacier National Park Research Library). (Right) A color-infrared aerial photo of the same area acquired in October 1980 (source: NASA/Glacier National Park). The mosaic of live and dead forest can be identified in both images. The letters correspond to the same area in each photo (A = stream confluence, B = small patch of live trees, surrounded by dead forest, C = linear ribbon of dead forest). See attached manuscript for full description of methods.

platform for future research of historical forest disturbance that would be very beneficial to the field of forest ecology.

In February 2014 we submitted a manuscript detailing our methods and findings to the journal *Remote Sensing of Environment*, where it is currently in review. A copy of the manuscript is attached to the report. Please do not distribute or cite the paper as it has not yet been published. The final product of this analysis is a model of mountain pine beetle severity in Glacier National Park (Figure 2). We were able to identify a gradient of mountain pine beetle mortality on the landscape using changes in satellite imagery reflectance over time. Our findings confirm that outbreak severity was significantly heterogeneous across the landscape.

We are now using this information to investigate the influence of mountain pine beetle mortality on fire severity. We are using GIS overlay analysis with our newly developed MPB outbreak severity map and maps of wildfire severity from the Monitoring Trends in Burn Severity data for all wildfires in the park between 1984 and 2006. Coupling these two data sets will allow us to gather additional information about the interaction of these two disturbances. For example, we can now calculate that 98% of the area that burned inside the park in the 1988 Red Bench Fire was impacted by some level of the mountain pine beetle outbreak. Of that area, 85% was impacted by mountain pine beetles as first detected in 1976. Moreover, we are comparing burn severity and mountain pine beetle outbreak severity to investigate how MPB outbreak severity interacts with wildfires to shape patterns of fire severity (Figure 3). Whereas it is only a single fire event, MPB-wildfire interactions in the Red Bench Fire indicate a positive relationship between MPB severity and fire severity. More specifically, forests that experienced no MPB outbreak or low-severity MPB outbreak experienced more low- and moderate-severity burned areas, and forests that experienced moderate- and high-severity MPB outbreak had more areas that experienced moderate- and high-severity fire. We are currently testing these relationships for all fires that burned in the study area to test if the relationships identified for the Red Bench Fire are consistent. Furthermore, we are testing if relationships between MPB and fire are contingent on the time interval between MPB outbreak and fire.

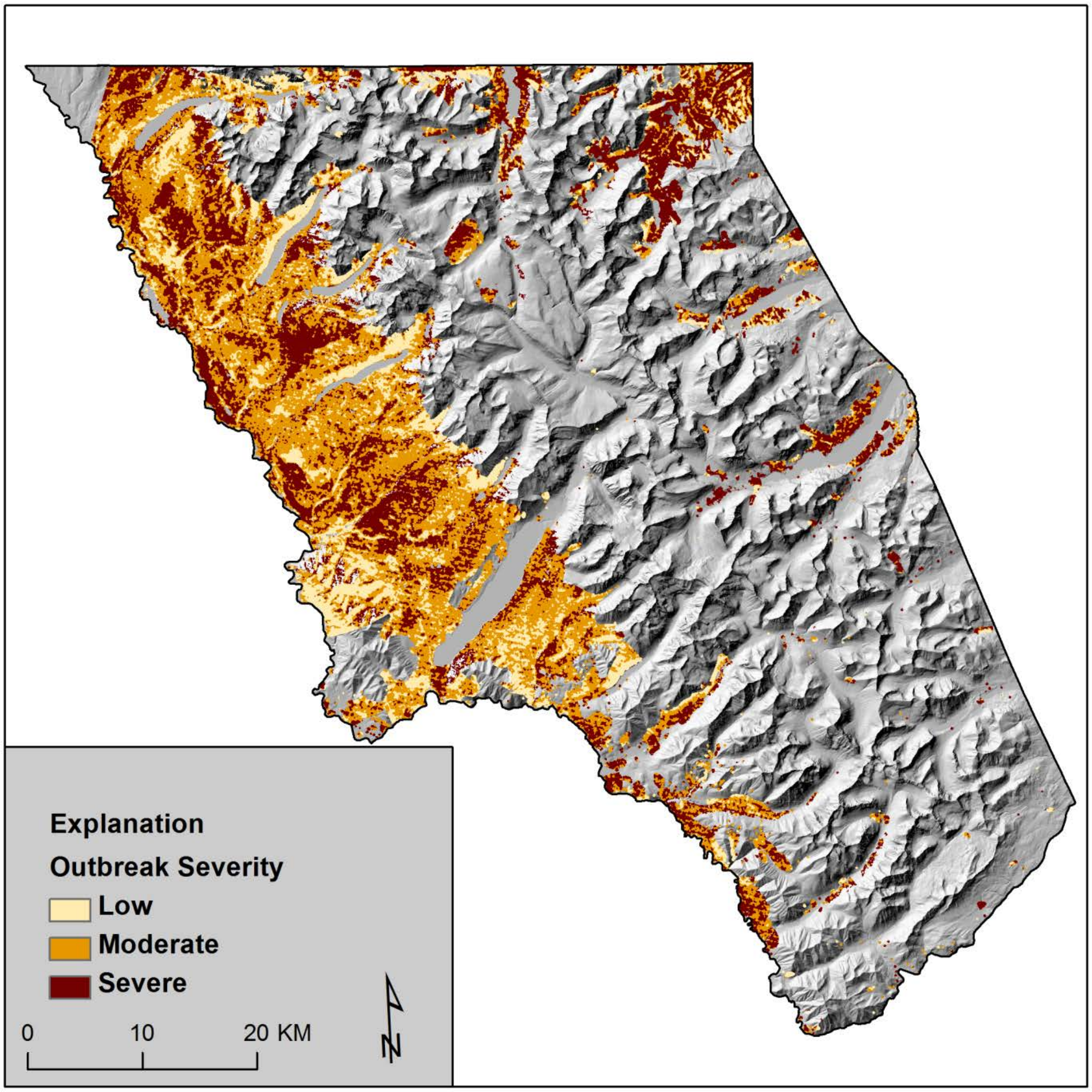

Figure 2. The output of the spatial model classified into three severity levels.

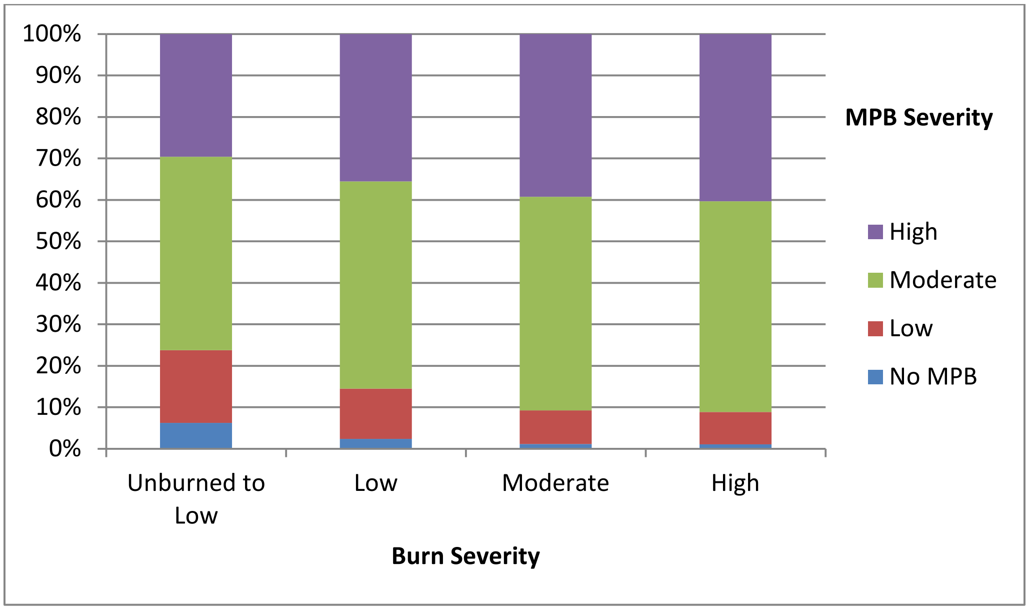

Figure 3. A comparison between the severity of the 1970s mountain pine beetle outbreak and burn severity of the 1988 Red Bench fire.

Manuscript in peer-review; please do not distribute

Modeling an Historical Mountain Pine Beetle Outbreak Using Multiple Lines of Evidence

TIMOTHY J. ASSAL[a, b*], JASON SIBOLD[c], and ROBIN REICH[d]

[a]Graduate Degree Program in Ecology, Colorado State University, 1401 Campus Delivery, Fort Collins, CO 80523, USA
[b]U.S. Geological Survey (USGS), Fort Collins Science Center, 2150 Centre Avenue, Fort Collins, CO 80526, USA
[c]Department of Anthropology, Colorado State University, 1787 Campus Delivery, Fort Collins, CO 80523, USA
[d]Department of Forest and Rangeland Stewardship, Colorado State University, 1472 Campus Delivery, Fort Collins, CO 80523, USA

Corresponding author at: USGS, Fort Collins Science Center, Fort Collins, CO 80526, USA.
Tel.: +1 970 226 9134.
E-mail address: assalt@usgs.gov (T.J. Assal).

ABSTRACT

Mountain pine beetles are significant forest disturbance agents, capable of inducing widespread mortality in coniferous forests in western North America. Various remote sensing approaches have assessed the impacts of beetle outbreaks over the last two decades. However, few studies have addressed the impacts of historical mountain pine beetle outbreaks, including the 1970s event that impacted Glacier National Park. The lack of spatially explicit data on this disturbance represents both a major data gap and a critical research challenge in that wildfire fire has removed some of the evidence from the landscape. We utilized multiple lines of evidence to model forest canopy mortality as a proxy for outbreak severity. We incorporate historical aerial and landscape photos, aerial detection survey data, a nine-year collection of satellite imagery and abiotic data. This study presents a remote sensing based framework to (1) relate measurements of canopy mortality from fine-scale aerial photography to coarse-scale multispectral imagery and (2) classify the severity of mountain pine beetle affected areas using a temporal sequence of Landsat data and other landscape variables. We sampled canopy mortality in 267 plots from aerial photos and found that insect effects on mortality were evident in changes to the Normalized Difference Vegetation Index (NDVI) over time. We tested multiple spectral indices and found that a combination of NDVI and the green band resulted in the strongest model. We report a two-step process where we utilize a generalized least squares model to account for the large-scale variability in the data and a binary regression tree to describe the small-scale variability. The final model had a root mean square error estimate of 9.8% canopy mortality, a mean absolute error of 7.6% and an R^2 of 0.82. The results demonstrate that a model of percent canopy mortality as a continuous variable can be developed to identify a gradient of mountain pine beetle severity on the landscape.

1. Introduction

Temperate forest ecosystems are subject to various ecological disturbances that can have profound effects on the structure of the ecosystem for many years after the event (Turner & Dale, 1998) and influence the likelihood, severity and spread of subsequent disturbances (Veblen et al., 1994). In western North America, native bark beetles are a major disturbance agent capable of regional-scale forest mortality (Raffa et al., 2008). Remotely sensed imagery has been used to characterize such widespread disturbance events over the last two decades (Wulder et al., 2006a). However, very little research has employed these techniques to study insect disturbance prior to the recent period of extended outbreak (~pre late 1990s). The northern Rocky Mountains experienced a widespread mountain pine beetle outbreak in the late 1970s to early 1980s (Logan & Powell, 2001). However, the lack of spatially explicit data on the extent and severity of this outbreak limits our understanding of the influence that this disturbance had on the landscape. To overcome this challenge, we utilized multiple lines of evidence to retrospectively characterize forest canopy mortality from the outbreak by comparing temporal changes in archived satellite imagery.

1.1 Mountain Pine Beetle Overview

The mountain pine beetle (*Dendroctonus ponderosae*) is a native species found in the western United States and Canada that attacks and reproduces in live trees (Bentz et al., 2010). The mechanisms with which populations switch to epidemic levels are complex (Bentz et al., 2010; Raffa et al., 2008), but include suitable host availability (amount, vigor, age and density) and condition (Fettig et al., 2007), along with beetle population survival and growth given thermal conditions (Powell & Logan, 2005). Epidemic populations are capable of landscape-scale forest mortality leading to cascading effects on forest structure, species composition and function (Raffa et al., 2008). Major host species include lodgepole pine (*Pinus contorta*), ponderosa pine (*P. ponderosa*), and whitebark pine (*P. albicaulis*) (Bentz et al., 2010). Impacted forests exhibit unique and visible characteristics at each stage of a mountain pine beetle attack (Wulder et al., 2006a). Killed trees begin to show visible changes as the foliage changes from green to yellow to red over the first year after the attack. The gray attack stage typically commences three years after the attack, as most trees will have lost all needles at that time (Wulder et al., 2006a).

1.2 Remote Sensing and Disturbance

Historical aerial photography is a valuable research tool providing detailed records of forest landscapes over the last half century or more. Although limited in spatial extent, these records provide a fine-scale snapshot of landscapes at one or multiple points in time. Previous studies have successfully used aerial photos collected during two or more time periods to measure changes in tree cover (Brown et al., 2006; Di Orio et al., 2005; Kadmon & Harari-Kremer, 1999; Kennedy & Spies, 2004; Manier et al., 2005; Platt & Schoennagel, 2009; Strand et al., 2006). The use of satellite multispectral imagery to map and monitor forest condition over larger regions is also well documented (Cohen et al., 2001; Maselli, 2004; Nemani et al., 2009; Schroeder et al., 2006; Townshend et al., 2012; Volcani et al., 2005) dating back to the early 1970s with the initiation of the Landsat program (NASA, 2013). Several studies have used aerial photos as a surrogate for field data collection and then used that information to scale up to satellite imagery. This technique has been accomplished to map various attributes including land cover type (Parmenter et al., 2003), tree cover (Carreiras et al., 2006; Cohen et al., 2001; Homer et al., 2007), and surface imperviousness (Homer et al., 2007). Photos can be used to sample post-disturbance forest patterns, such as canopy mortality. The aerial photo reference data can be used to bridge the gap in scale between localized tree mortality measures and the more coarse scale of satellite imagery (Meddens et al., 2013). This hybrid approach allows for detection of fine-scale disturbance patterns captured in the aerial photos, while taking advantage of the multispectral and multitemporal components of Landsat imagery at the landscape scale. Furthermore, it provides a pathway to conduct a retrospective analysis.

Ecological disturbance alters ecosystem structure by both abrupt, conspicuous change and by gradual, slow change over some period of time. Such impacts allow remote sensing to capture the pre- and post-landscape, and in some cases, the duration of the event. Aerial photos have been utilized to investigate the impacts of fire (Bebi et al., 2003; Johnson & Fryer, 1987), insect damage (Bebi et al., 2003; White et al., 2005), extreme drought (Allen & Breshears, 1998), and blowdown (Baker et al., 2002) on forest and woodland ecosystems. At regional scales, multispectral satellite imagery has been employed to study diverse types of forest disturbance including fragmentation (Fuller, 2001), fire (Turner et al., 1994), drought (Huang et al., 2010) and insect induced mortality (DeRose et al., 2011; Vogelmann et al., 2009). Numerous studies have utilized multispectral imagery to document the extent and severity of the recent mountain pine beetle outbreak over the last decade. Efforts range from fine-scale satellite and aerial multispectral imagery acquired from one time period (Coops et al., 2006; Dennison et al., 2010; Hicke & Logan, 2009; Meddens et al., 2011), to moderate resolution sensors incorporating multiple time periods (Goodwin et al., 2008; Meddens et al., 2013; Meigs et al., 2011; Wulder et al., 2006b).

We found few studies in the literature that used the first generation of Landsat data to detect mountain pine beetle outbreaks or other insect-driven forest disturbance. The Landsat Multispectral Scanner System (MSS) sensor was carried onboard the first five Landsat satellites and provided imagery from 1972 until 1995 (NASA, 2013). Researchers in British Columbia (Harris et al., 1978) used single date MSS imagery to detect damage caused by the Douglas-fir tussock moth and western spruce budworm with little success. Weber et al. (1975) employed single date MSS imagery to map mountain pine beetle damage in Ponderosa pine. Rencz and Nemeth (1985) tested both a single date approach and a change detection approach over a six-year period to map mountain pine beetle damage in British Columbia. Both mountain pine beetle studies concluded that MSS imagery does not have the capability to detect beetle damage given the spatial resolution of the imagery. However, the British Columbia study (Rencz & Nemeth, 1985) noted greater detection accuracy at sites with heavy, continuous damage, suggesting the spatial resolution is less limiting in areas with high-severity outbreaks.

1.3 Outbreak Impacts to Forest Vegetation Spectral Properties

Living vegetation absorbs blue and red light energy, while radiation in the green and near-infrared portion of the electromagnetic spectrum is reflected (Jones & Vaughan, 2010). Therefore, color-infrared photos can be used to distinguish between areas of live trees and dead trees. As the foliage of killed trees changes during the first year after the attack, the spectral response also begins to change (Rencz & Nemeth, 1985). At the cellular level, mortality contributes to a reduction in foliar moisture and chlorophyll, as other pigments and cellular structure begins to break down (Mauseth, 1988). As a result, the spectral reflectance in the red wavelength (630-690 nm) increases, whereas the reflectance in the green wavelength (520-600 nm) decreases (Ahern, 1988).

Disturbances where large portions of forest vegetation are removed from the landscape, such as fire and clear cutting, create a drastic change in spectral reflectance. Conversely, subtle changes in foliage color associated over time may prove more difficult to detect. Nevertheless, the phenology associated with mortality caused by an outbreak will lead to a change in satellite-detected reflectance of the forest canopy. An analysis of multiple years of moderate spatial resolution imagery has the potential to capture reflectance patterns before, during and after landscape-scale disturbance events (Goodwin et al., 2008; Wulder et al., 2006a).

Multiple types of spectral indices have been employed to detect the impacts of mountain pine beetle disturbance over the last decade. Examples of indices include the Normalized Difference Moisture Index (Goodwin et al., 2008, 2010; Meddens et al., 2013), the Tasseled Cap (Meddens et al., 2013), the Enhanced Wetness Disturbance Index (Skakun et al., 2003; Wulder et al., 2006b), the Normalized Burn Ratio (Meigs et al., 2011), the Red-Green Index (RGI) (Coops et al., 2006; Hicke & Logan, 2009; Meddens et al., 2013), the Band 5/Band 4 Ratio (Meddens et al., 2013), and the Normalized Difference Vegetation Index (Meddens et al., 2013). Various levels of success were obtained with each index. Many of these indices are derived from Landsat TM or ETM+ imagery. However, Landsat TM imagery is not available prior to 1984 and Landsat ETM+ imagery is not available before 1999. Because the outbreak that is the focus of this study erupted in the mid-1970s, Landsat MSS imagery represents the only available satellite imagery. Given the four multispectral bands of MSS (Table 1), we were only able to utilize a subset of these indices.

1.4 Aerial Detection Survey Data

The US Forest Service (USFS) has been conducting annual forest health aerial detection surveys (ADS) since the middle of the 20th century. In summary, human observers record the type and extent of abiotic and biotic disturbances and host species onto sketch maps (Meigs et al., 2011). The sketch maps are hard copy maps used by human observers in planes that are later converted to digital form. This data has successfully been integrated into remote sensing detection studies of insect disturbance (Meddens et al., 2012; Meigs et al., 2011). The Forest Health Protection Aviation Program in USFS Region 1 (including Glacier National Park) maintains digital files of the ADS data since 2000. Staff at Glacier National Park digitized the ADS data from 1962-1998. The data include information about insect species, host tree species, damage type, and forest type. However, very few polygons contained information on the number of trees killed per acre (severity), which is commonly included in contemporary ADS data and is critical to relating outbreaks to forest processes and change. Furthermore, the disturbance polygons identified in the ADS data were very large (e.g. > 70,000 ha). Although useful for broad-scale monitoring, we suspect the ADS data does not represent the heterogeneous impacts of the disturbance. Since we are interested in both the extent and severity of the disturbance, these missing details heavily influenced the direction of this study.

1.5 Objectives

The goal of the study was to test an approach combining multiple lines of evidence to reconstruct the extent and severity of a mountain pine beetle outbreak in a topographically complex landscape. Furthermore, subsequent disturbance (fire) has removed evidence from large areas of the study area. To accomplish this, we used a combination of aerial detection survey data, historical aerial and landscape photos, National Park Service reports and a temporal sequence of satellite imagery. Each data source has limitations in the spatiotemporal record. However, by combining disparate sources of data across spatial and temporal scales, we aimed to reduce the uncertainty associated with reconstructing outbreak parameters. Employing multiple lines of evidence from independent data sources has the potential to extend the information associated with each piece of data and create a robust composite picture of the outbreak (Swetnam et al., 1999). Reference data was collected from aerial photos and scaled up to satellite imagery measurements over time. We hypothesized that the impacts of the disturbance to the forest canopy (i.e. mortality) would be captured in spatiotemporal changes in reflectance. Finally we sought to demonstrate a novel approach in the use of existing data to assess an historic disturbance.

The objectives of this study are to:

1. Relate measurements of canopy mortality from fine-scale aerial photography to coarse-scale multispectral imagery;
2. Classify the severity of mountain pine beetle affected areas using a temporal sequence of Landsat data and other landscape variables.

2. Methods

2.1 Study Area

The study was located in Glacier National Park in northwestern Montana, USA (Figure 1). The area was chosen because of the extensive mountain pine beetle epidemic that occurred there in the 1970s (Hamel et al., 1977; McGregor et al., 1975). The park encompasses 4,080 km^2 (408,000 ha) of diverse terrain on either side of the Continental Divide. Mean average annual precipitation is 73.1 cm, and average annual maximum and minimum temperatures are 11.9 ºC and -0.2 ºC, respectively (1971-2000) (Western Regional Climate Center, West Glacier station, elevation: 970 m, http://www.wrcc.dri.edu; accessed 17 December 2012). The climate averages from this station are consistent with stations on the east side of the park. Elevation ranges from ~ 950 m to 3184 m above sea level and major cover types include grasslands, conifer and deciduous forests, lakes, wide glacial valleys and steep alpine zones. Forests are dominated by lodgepole pine (*Pinus contorta*), western larch (*Larix occidentalis*), Engelmann spruce (*Picea* engelmannii) and Douglas-fir (*Pseudotsuga menziesii*).

Given the size and diverse landscape of the park, we limited the study area based on several assumptions. First, vegetation cover types not susceptible to mountain pine beetle attack were identified using ReGAP (Davidson et al., 2009) and omitted. Second, we calculated the cumulative extent of mountain pine beetle damage identified by the ADS data between 1971 and 1987. The area not impacted by the mountain pine beetle outbreak during the buffered time period was omitted from further analysis. The area of interest was also confined by the extent of available satellite imagery used in the analysis. The confined area of interest is 1195 km^2 (119,552 ha) and ranges in elevation from ~ 950 m to 2960 m above sea level (Figure 1).

2.2 Aerial and Landscape Photograph Processing

Six color infrared aerial photographs were obtained in digital format from the US Geological Survey's Earth Resources Observation and Science Center (Figure 1). Four of the photos were acquired in 1982 (west of the Continental Divide), two in 1984 (east of the divide). All photos have a scale of 1:58,000 and were scanned at a resolution of 1800 dots per inch. The photos were orthorectified to a 2009 NAIP photo (National Agriculture Imagery Program) using numerous ground control points (GCPs) and a 30 m digital elevation model (DEM). The average root mean square error (RMSE) for each photo was less than two meters. We independently assessed the average displacement between each of the orthorectified images and the 2009 NAIP image at multiple locations within each image pair. The average displacement between both sets of images was less than two meters and deemed acceptable. The orthorectification was accomplished using the Leica Photogrammetry Suite (LPS) (Erdas, Inc., Norcross, GA, USA).

We searched two landscape photographic archives in an effort to locate additional sources with evidence of the disturbance. The US Geological Survey's Photographic Library contains hundreds of photographs of Glacier National Park, dating back more than 100 years.

Unfortunately there were no photos from the 1970s and 1980s that captured any apparent stage of the outbreak. However, the Glacier National Park Research Library contained several color photos taken in the late 1970s or 1980 that contained evidence of the outbreak. In several cases the extent of the aerial color infrared photo and the color landscape photo were congruent. We were able to match the two photos and identify unique patterns and patches of mortality in each photo. Although this was a qualitative analysis, the additional information provided us with concrete evidence of the disturbance in the aerial photos (Figure 2).

2.3 Aerial Detection Survey Data

Glacier National Park supplied us with a digital version of the ADS data from 1962-1998. We subset annual shapefiles from 1971 to 1987 since this corresponded with the start of the outbreak and the last year before extensive fires in the park (1988). We queried polygons associated with mountain pine beetle using the *Damage Causal Agent* attribute code and clipped the shapefile to the extent of the park for each year. Each annual shapefile was converted to an annual grid (30 m) and snapped to the master Landsat image. The grids were aggregated to form a cumulative mountain pine beetle extent and used to constrain the study area. We did examine the ADS data for other disturbance agents within the park to ensure there were no unaccounted disturbances. However, we found very few disturbance polygons, accounting for a very small area, within the analysis mask.

2.4 Satellite Image Processing

We conducted a search of the US Geological Survey's EarthExplorer archive (USGS, 2012) to acquire relatively cloud-free scenes of the study area before, during and after the peak of the outbreak. We acquired 24 Landsat Multispectral Scanner System (MSS) scenes for preliminary evaluation. However, many of the scenes contained clouds, were acquired too early or late in the growing season or contained striping in the data. We retained nine scenes to be used in the investigation (Table 2). Late summer data were used (late August-September) due to availability of cloud-free imagery and the presumed relative phenological stability of the forests during this time period (Vogelmann et al., 2009). All of the scenes were preprocessed by the US Geological Survey to level 1T (terrain corrected data) and therefore we did not apply a topographic normalization. MSS imagery has a spatial resolution of 60 m in four spectral bands (Table 1).

Twenty GCPs were established to compare the spatial accuracy between the 2009 NAIP photo and a 2010 Landsat Thematic Mapper (TM) image of the study area. We used the AutoSync module in Erdas Imagine to georectify the image to the 2009 photo (RMSE < 0.5 pixel). This process was then repeated to georectify each of the 9 Landsat MSS images to the 2010 TM image. Each MSS image had an RMSE < 0.4 pixel and was resampled in AutoSync during the georectification process. The MSS images were resampled to 30 m using a nearest neighbor transformation to minimize geometric offsets in the image stack (Goodwin et al., 2008). However, the spatial resolution of the data is still considered 60 m.

Radiometric calibration of imagery is an important step for creating a consistent, high-quality temporal image series for use in change detection analysis. We converted the four bands of each image from Digital Numbers to absolute units of at-sensor spectral radiance using the formula (Chander et al., 2009):

$$L_\lambda = (LMAX_\lambda - LMIN_\lambda / Q_{calmax} - Q_{calmin}) * (Q_{cal} - Q_{calmin}) + LMIN_\lambda \qquad (1)$$

where

L_λ = Spectral radiance at the sensor's aperture [W/(m^2 sr µm)]

Q_{cal} = Quantized calibrated pixel value [DN]

Q_{calmin} = Minimum quantized calibrated pixel value corresponding to $LMIN_\lambda$ [DN]

Q_{calmax} = Maximum quantized calibrated pixel value corresponding to $LMAX_\lambda$ [DN]

$LMIN_\lambda$ = Spectral at-sensor radiance that is scaled to Qcalmin [W/(m^2 sr µm)]

$LMAX_\lambda$ = Spectral at-sensor radiance that is scaled to Qcalmax [W/(m^2 sr µm)]

The spectral radiance values were converted to Top-Of-Atmosphere (TOA) reflectance to account for differences in sensor and viewing angle using the formula (Chander et al., 2009):

$$\rho_\lambda = \pi * L_\lambda * d^2 / ESUN_\lambda * \cos\theta_s \qquad (2)$$

where

ρ_λ = Planetary TOA reflectance [unitless]

π = Mathematical constant equal to ~3.14159 [unitless]

L_λ = Spectral radiance at the sensor's aperture [W/(m^2 sr µm)]

d = Earth-Sun distance [astronomical units]

$ESUN_\lambda$ = Mean exoatmospheric solar irradiance [W/(m^2 µm)]

θ_s = Solar zenith angle [degrees]

All scenes were processed by the USGS using the Level 1 Product Generation System (LPGS) and therefore included a header file (.MTL). Inputs used in the formulas above were supplied by the header file for each scene and Chander et al. (2009).

Each image was then snapped to the reference image (1979 image) in ArcGIS to ensure that each 30 m pixel for every year was exactly congruent with the master image. An absolute normalization was applied to the 1979 master image using a dark object subtraction technique (Chavez 1988). The minimum pixel value of each band (recorded in at least 1000 pixels), representing deep glacial lakes and shadows, was identified (Chavez, 1996). The theoretical radiance of a dark object is assumed to have 1% reflectance (Chavez, 1996; Moran et al., 1992) so the minimum identified pixel value was multiplied by 0.99 to generate the presumed dark object of each image band.

The remaining images were normalized to the master image using a relative normalization technique. This procedure removes non-surface noise and improves the temporal homogeneity between images so that spectral change associated with surface phenomena can be detected (Yuan & Elvidge, 1996). Psuedo-Invariant Features (PIFs) are targets in each image that are not expected to change between image dates (Schott et al., 1988). Relative normalization is based on the assumption that a linear relationship exists between the reference image and the image to be normalized (Schott et al., 1988; Yuan & Elvidge, 1996). This technique has been applied in many studies to analyze vegetation change (Bradley & Fleishman, 2008; Schroeder et al., 2006; Vicente-Serrano et al., 2008). We identified 60 PIFs that encompassed a range of pseudo-invariant reflectance values in each band. Each PIF was 32,400 m^2 in size; equivalent to a 3x3 block of 60 m Landsat MSS pixels. The mean of the reflectance values at these sites were used to fit an ordinary least squares regression model between the image to be normalized for each year and the reference image for each of the four bands. We tested the residuals for spatial autocorrelation using the Moran's I statistic and the Likelihood Ratio Test (Legendre & Fortin, 1989). If spatial autocorrelation was detected, a spatially autoregressive model was used to fit the data (Cressie, 1993). In all cases, the fit of lines used to spectrally align the images had R^2 values > 0.92. Statistical analysis was conducted using the r package (R Development Core Team, 2011) and the linear regression was applied to each image in Erdas Imagine.

Given the four multispectral bands of MSS, we were only able to utilize three spectral indices in the model evaluation process (Table 3). The GNDVI is sensitive to the presence of chlorophyll since the green spectral region is used instead of the red region (Carreiras et al., 2006). We did not use Band 3 as a covariate as it is often highly correlated with band 4 of MSS data. A preliminary investigation identified that NDVI performed the best among spectral indices. In an effort to limit redundancy in the data, we transformed the NDVI time series using principal component analysis. The principal components were used as predictor variables in one of the five models tested.

2.5 Sampling

We estimated beetle induced forest mortality using data collected from the aerial photos and compared these measurements with changes in spectral values over time. We segregated the landscape into 12 different facets based on slope and aspect. These two variables influence forest composition, tree vigor and subsequent susceptibility to mountain pine beetle (Raffa et al., 2008). Furthermore, dividing the landscape into sub-regions of similar biophysical characteristics can isolate spectral gradients (Homer et al., 2004). Both variables were derived from the elevation dataset. Aspect was classified into four categories (north, east, south or west) while slope was classified into three quantiles: low (<12%), moderate (12-29%) and high (>29%). Initially 350 random points were proportionally allocated in each of the 12 landscape classes, and square plots of 180 m x 180 m were delineated around the center of each point. The plot size was chosen considering the spatial resolution of the satellite imagery, i.e. 3 x 3 Landsat MSS pixels. A negative buffer was used to insure that plots were located completely within one landscape facet. Many of the initial plots were deleted (10%) because they did not completely fall within a landscape facet. In addition, limitations due to topographic shadow or image blur from the orthorectification process warranted the omission of some plots (13%). As a result, each landscape facet did not contain the same number of sampling plots.

An unsupervised classification in Erdas Imagine was conducted on each air photo resulting in 20 classes. We used an iterative approach to determine the number of unsupervised classes that maximized spectral separation without generating an unwieldy number of classes. For each plot, we manually interpreted the 20 classes and assigned each class to live forest, dead forest, or shadow (Figure 3). We then calculated the ratio of dead canopy cover to total canopy cover in each plot. We omitted shadow pixels as they represent unknown cover types.

2.6 Statistical Analysis

Regression analysis can be used to explain large-scale variability, while model residuals can be used to describe small-scale variability in the data (Cressie, 1993). We used a generalized linear model (GLM, Gaussian distribution, Identity link function) to identify a set of explanatory variables to estimate canopy cover change on the sample plots over time. Predictor variables included spectral indices derived from nine years of Landsat MSS data, topography (elevation, slope, aspect and topographic position index), and variables derived from the ADS data (first year detected, last year detected and total number of years detected). Aspect and the variables derived from the aerial survey data were treated as indicator variables in the analysis. Aspect was binned into four classes: North (0-45º; 315-365º), East (45-135º), South (135-225º), and West (225-315º). Three categorical variables were derived from the aerial survey data: first year of attack (early, mid, or late in the outbreak), last year of attack (early, mid, or late in the outbreak) and total number of years recorded during the outbreak (low, moderate, or high).

We tested five models in our analysis using different combinations of vegetation indices as the primary biotic variables. For each model, a stepwise selection by Akaike's Information

Criterion (AIC) was used to identify the best subset of independent variables to include in the regression models (R Development Core Team, 2011). The aspect variable was allowed to interact with the primary vegetation index in each model. We evaluated the models through consideration of AIC, the mean absolute error of prediction (MAE) and the root mean square error of prediction (RMSE). Furthermore, a ten-fold cross validation procedure (DAAG package in R) was employed to calculate the prediction error of each model.

Residual error from the regression model can be utilized to describe the small-scale variability in the data (Manier et al., 2005; Reich et al., 2011). We modeled the residual error from the selected regression model using a binary regression tree. We tested the residuals of the selected GLM model and the regression tree model for spatial autocorrelation using the Moran's I statistic (Legendre & Fortin, 1989). The sampled plots were clustered on the landscape into three distinct groups based on the availability of the aerial photos. We assumed points between each cluster were spatially independent and employed a block diagonal spatial weights matrix (Upton & Fingleton, 1985) to account for the clustered nature of the plots.

The residuals of the GLM-CART model exhibited spatial autocorrelation. We addressed the issue by running the regression analysis using a Generalized Least Squares (GLS) model. A variogram was fit using the residuals of the GLM model to describe the degree of spatial dependence in the residuals. A Gaussian variogram model was fit to the sample variogram using least squares to estimate the nugget, sill and range. The GLS regression was used to estimate the parameters of the trend surface model in the presence of spatial autocorrelation. We allowed plot location (east or west of the Continental Divide) to enter the model to test if the outbreak impacts were different on either side of the divide.

After parameterizing and validating the models, forests canopy change was projected to the landscape area of interest in three steps. First a trend surface was created from the parameters of the GLS model using the raster calculator in ArcGIS. Next, a surface of the residuals generated from the regression tree model was created using a series of conditional statements in the raster calculator. Finally, the trend and residual surfaces were added together to create a continuous surface of forest canopy change scaled between 0 and 1. Areas of cloud cover, cloud shadow and topographic shadows represent uncertainty and were omitted from the analysis. Only two years of data (1978 and 1983) contained sparse clouds, but topographic shadows were present in all years. We applied a NDVI threshold (< 0.2) to remove clouds and topographic shadows (Hicke & Logan, 2009) and cloud shadows were manually delineated and removed.

3. Results

3.1 Aerial Detection Survey Data

Our analysis of the aerial survey data indicates the outbreak was first identified in 1971 in the north-west portion of the park in very small isolated patches. The outbreak continued to spread from these centers until the mid-1970s when it was reported widely across the western portion of the park (Figure 4). There was no data available for 1975, and the following year the area affected by beetles significantly expanded on the western side of the park. The aerial survey continued to report large areas impacted from 1977 through 1980. The outbreak was first identified east of the Continental Divide in the north central and north east portion of the park in 1979. In the early 1980s, the area affected by beetles quickly decreased (Figure 5).

3.2 Determination of Tree Canopy Cover

A total of 267 plots were used to estimate tree canopy mortality from the air photo analysis (Table 4). Initially, 282 plots were analyzed, but 15 were removed from the data set because the photo plots fell within topographic shadows, cloud cover or cloud shadows in the satellite imagery. The study area is dominated by west facing slopes, followed by south, east and north. Each aspect class did not contain the same number of plots (see Section 2.5). However, the number of plots in each aspect class is an adequate reflection of the percentage of the study area in each aspect class. Plots ranged from very little mortality (4.4%) to nearly complete mortality (99.8%). West-facing plots had the highest mean mortality (68.3%), while plots in the east aspect class had the lowest mean mortality (49.4%) (Table 4). The majority of the data is concentrated in mortality classes ranging from 40-90% (Figure 6). Given the severity and extent of the outbreak, this is not an unexpected finding.

3.3 Model Adjustment and Validation

The model that employed NDVI and the Green Band (NDVI+G) (Table 5) provided the best estimation of canopy change over time. This model had the lowest AIC (-237.55), MAE (10.8%), and RMSE (13.6%) values while accounting for the greatest amount of explained variability (65.4%) (Table 5). Furthermore this model had the lowest prediction error (15.4%) of any model from the cross validation procedure. The incorporation of a green band resulted in a stronger model than using NDVI alone (Table 5). The NDVI and PCA models had identical coefficients of determination, and similar MAE and RMSE. However, the PCA model had substantially higher prediction error. The GNDVI model did not perform as well as the three NDVI based models and the red-green index proved to be a poor indicator of mortality.

The NDVI+G model was selected to describe the large-scale variability of canopy change over time. However, the residuals of the GLM model exhibited spatial autocorrelation (Moran's *I* test; $p < 0.0001$) indicating that the null hypothesis of spatial independence in the residuals be rejected. The variables included in the NDVI+G model were then analyzed using a GLS model that explained 62% of the variability with higher MAE (18%) and RMSE (21.1%) than the GLM model (Table 6, Figure 7). However, the residuals of the GLS model did not exhibit spatial autocorrelation (Moran's *I* test; p =0.64). The green band from 1978 was the most important predictor west of the Continental Divide, with a relative contribution to the model of 10.7%. The green band from 1987 was the most important predictor east of the divide, with a relative contribution to the model of 11.8%. Decreased values of green band reflectance indicated a substantial increase in canopy mortality. NDVI from 1977 and 1981 were highly significant in the model on the west side of the park ($p<0.001$) and also exhibited a negative relationship with canopy mortality. NDVI from 1977 was also significant on the east side of the park.

The residuals were used to model the small-scale variation in the data using binary regression trees. The initial regression tree identified 27 nodes and location (east or west of divide) did not enter the analysis, so one tree was used to fit both sides of the Continental Divide. Given that regression trees are prone to overfitting, we conducted a 10-fold cross validation on the data and subsequently pruned the tree to 22 nodes. This simplified the model while still accounting for spatial autocorrelation. The combined model (GLS + CART), which captures both the large- and small-scale variability, had a lower rate of MAE (7.6%) and RMSE (9.8%) than the GLS model. The combined model increased the amount of explained variability in the data by nearly 20% (R^2 = 0.819) (Figure 8). The residuals of the combined model are spatially independent (Lagrange multiplier test; p=0.27) and the standardized mean square error (SMSE) of the combined model is 0.996. An SMSE value of one indicates consistency between the estimation error variance and the observed error variance in the model (Hevesi et al., 1992).

The combined model was then applied spatially to the study area as a continuous surface with modeled canopy cover change scaled between 0 and 1. We binned the modeled data into three categories based on natural breaks in the data (Figure 9). This classification resulted in 20% of the project area in the low category (< 0.37 canopy change), 46% in the moderate and 34% in the severe category (>0.62 canopy change). Pockets of high severity are found throughout the park across the elevation gradient present. The three classes are generally represented across the study area. However, it should be noted that pockets of low and severe impacts are clustered, with the moderate severity often forming a transition between the classes.

To provide perspective on the classification, a color-infrared photo and corresponding classification map is shown in Figure 10. Based on these visual comparisons, our model appears to capture high levels of mortality associated with beetle attack areas as well as areas not as heavily impacted. Furthermore, the gradient of impact on the landscape appears to be well represented in the model. Example spectral trajectories of the three classes show clear delineation during extent of the outbreak (Figure 11).

4. Discussion

A primary objective of our analysis was to develop a methodology to reconstruct the extent and severity of the outbreak. We were able to identify a gradient of mortality on the landscape using changes in NDVI and the green band reflectance over time. Our findings confirm the outbreak was not homogenous across the landscape (Figure 9). The reported error metrics are reasonable given limitations in the data and comparable to related studies of insect impacts on the forest canopy (Townsend et al., 2012). Error associated with the ADS data was not quantified. Furthermore, this information was collected by observers presumably working under difficult conditions. Therefore we suggest our model represents an unbiased view of the disturbance. In addition, the modeling framework we applied in this study should be transferable to other areas with similar forest disturbance characteristics.

This study builds on the ideology of many of the aforementioned studies which used remotely sensed data to document various stages of the late 1990s-mid 2000s mountain pine beetle outbreak. The common theme is the development of a time series imagery stack to assess spectral changes over time (Goodwin et al., 2008; Meddens et al., 2013; Meigs et al., 2011). However, we were unable to utilize many of the vegetation indices (e.g. Normalized Difference Moisture Index) used in these studies. Given that our study objectives hinged around an historic disturbance that occurred in the mid-1970s and early 1980s, we were unable to use imagery with the spectral resolution needed for many of those indices. The major difference in our study and those described in section 1.3, is that the disturbance we are interested in occurred in the 1970s and early 1980s. This predates the advent of Landsat TM/ETM+ imagery and other finer scale imagery employed in those studies.

There were two main differences between our study and those that used MSS data (Harris et al., 1978; Rencz & Nemeth, 1985; Weber et al., 1975). First, we attempted to capture the gradient of the disturbance on a continuous scale between 0 and 1. Second, we employed multiple time periods of imagery to assess spectral changes at sites over time. Although Rencz and Nemeth (1985) used a change detection procedure, there was a gap of six years between images. The use of just two images was likely insufficient to capture the full range of phenology associated with the disturbance from pre-attack through the green, red and gray stages, followed by the likely expansion of understory growth following canopy mortality. Conducting a retrospective analysis afforded us several advantages over the prior MSS studies. The Landsat archive is now readily available at no cost, removing the financial burden that inhibited prior investigators from developing a time series imagery stack (Woodcock et al., 2008). Furthermore, advances in radiometric calibration provide a basis for standardized comparison between images acquired on different dates and by different sensors (Chander et al., 2009).

There are several strengths associated with our study that allowed us to overcome numerous limitations. Overall, we provide an objective framework that can be applied to other areas, at other time periods, involving other types of forest disturbance. The major limitation of quantifying a disturbance over a large, topographically complex landscape where subsequent fire has erased some of the evidence was overcome using existing data that has been archived for a number of years. The remote sensing archive allowed us to extract information about the condition of the forest canopy across spatiotemporal scales. By employing multiple lines of evidence, each independent data source contributed to a composite picture of the disturbance (Swetnam et al., 1999). Several key factors led to a successful analysis. The first was employing a mask to restrict the area of analysis (Garrity et al., 2013) to forest types where mountain pine beetle had the potential to impact. The second critical element was the development of a normalized time series of reflectance (Townsend et al., 2012; Vogelmann et al., 2012) to characterize changes over time. We obtained many more images (24) than we ultimately used (9), but this was necessary to conduct an exhaustive evaluation of available imagery. The consistent level of pre-processing performed on the imagery by the USGS and our procedure to convert data to at-surface reflectance aided in the success. Furthermore, the image acquisition dates were within a six-week window, which limited intra-year differences. The final critical element was the development of a novel approach to measure mortality in available aerial photos and scale up to multiple years of satellite imagery. This procedure was crucial given the absence of field data.

4.1 Ecological Considerations

In areas where mountain pine beetle disturbance induces high mortality in the forest canopy over a short time period, there will be a relatively quick change in NDVI. Therefore these areas will have a heightened chance of detection by remote sensing methods. In addition, the release of light, nutrients and moisture will occur at one time period. Therefore the flush of understory growth will likely occur over a relatively short time period. This increases the likelihood of obtaining a tight sequence of images to detect these rapid changes. Given the high severity of the impact, the model identified large negative relative contributions of the green band in the 1970s on the west side of the divide, indicative of an increase in canopy mortality. However, the 1987 green band was significant, with a large positive relative contribution to the model. This can be interpreted ecologically in that there was a sharp increase in canopy mortality during the late 1970s, but understory growth was prevalent in these high severity areas by the late 1980s. The outbreak moved from the west to east over the divide. The 1987 green band had a large negative contribution to the east side model, suggesting recent canopy mortality dominated the spectral signature, while understory regrowth was likely not widespread.

However, the impacts of mountain pine beetle disturbance on the forest canopy do not always exhibit characteristics that are easily identified by remote sensing methods. Areas that have lower amounts of mortality will be composed of a mix of live and dead trees resulting in a gradient of mortality over the duration of the disturbance. As trees die over this time period, they will likely be interspersed with live trees. Given that the spectral response of a pixel is an amalgamation of all elements present (Lefsky & Cohen, 2003), there will be a smaller change in reflectance. Additionally, as individual trees die, the release of resources will impact a smaller area of understory regrowth. The localized understory regrowth could offset or suppress the change in reflectance associated with canopy mortality. This problem is manifested on the landscape as the cycle of canopy mortality, resource release, and understory flush could be occurring simultaneously in localized areas.

Several ecological phenomena could pose challenges to this methodology, particularly if the recent disturbance history of the study area is unknown. Other disturbances could be identified by this method, without being attributed to mountain pine beetle. We were able to incorporate ancillary data about the mountain pine beetle outbreak such as ADS data, park reports and knowledge from park staff to supplement the primary imagery method. Harvest events typically have sharp geometric boundaries (Goodwin et al., 2008) that often persist in reflectance patterns for quite some time after the event. Unknown fires that are low severity or small in area could be difficult to segregate from insect disturbance mortality, particularly if the event corresponds with a gap in satellite imagery. Other insect disturbances such as mortality or defoliation events in the study area could be detected as well (Meigs et al., 2011; Townsend et al., 2012). We analyzed the *Damage Causal Agent* attribute code of the aerial survey data and found nearly no other disturbance types recorded within the study area during the time periods 1971-87. Given that our objective was to detect landscape-scale mortality associated with a widespread, high-severity disturbance, we were not concerned with these small disturbances.

Periods of drought and fluctuations in hydrologic year (Oct.-Sept.) precipitation could impact inter-annual indices of vegetation reflectance in areas of low mortality. However, our normalization procedure should account for some of these differences between imagery years. The establishment of appropriate reference conditions of an area remains a challenge in ecological studies (Millar et al., 2007). Finally, all of the aforementioned challenges are made more complex when attempting to conduct a retrospective analysis of historical forest disturbance.

4.2 Technical Considerations

The technological challenges associated with this study are centered on the spatial, temporal and spectral resolution of the aerial photographs and satellite imagery. Although we were constrained to the use of best available data for the time period, consideration of some of the shortcomings is necessary. We used aerial photographs collected in 1982 (four) and 1984 (two). The scale of each photograph (1:58,000) was relatively coarse. This scale does not allow for the identification of an individual tree crown. However, we believe the size of the photo plots (180 m x 180 m) was adequate to characterize the level of mortality within a stand. Given that our objective was to measure canopy mortality, we were confined to using color-infrared photographs. We would have considered natural color photographs if they had been available in the archive. There were additional photographs available in the archive that were not selected due to a combination of acquisition date, coarse resolution and gray scale film. Although nominal, there are acquisition costs associated with historic aerial photos, and the orthorecticfication process can be time consuming.

Additional landscape photographs would have been extremely helpful. However, we were limited by those that were taken by park staff at the end of the outbreak and housed in the National Park Service archive. Although they were not used in a quantitative analysis, they provided valuable evidence of the impact of disturbance.

The Landsat MSS imagery employed in this study is also subject to spatial, temporal and spectral constraints. Although we resampled the MSS imagery from 60 to 30 m to aid in the georectification process, we still considered the spatial resolution to be 60 m. Pixels represent an amalgamation of all spectral properties of elements found within a 60 x 60m footprint on the ground (Lefsky & Cohen, 2003). Therefore the spatial resolution of MSS imagery is limiting to the amount of mortality that can be detected at one pixel between multiple time periods. As a result, areas that experienced low mortality may have been underestimated by our model. The temporal limitations of the image archive are two-fold. The study may have benefited from a higher frequency of images collected every calendar year. Also, it would have been preferable to have additional image years to establish pre-outbreak conditions. However, it was not tenable to alleviate these constraints given the available imagery and the timing of the disturbance. The spectral resolution of MSS imagery is limited compared to TM/ETM+ imagery. Many of the indices that have been successfully applied to recent outbreaks are developed from a wider spectral range than that of MSS. All of these factors may limit the sensitivity of the study to detect different levels of mortality, especially low levels of mortality. However, given the scale and severity of the disturbance, coupled with the dense imagery stack that was assembled, we were still able to achieve acceptable results.

The Tasseled Cap transformation for Landsat data has been used to distill information from Landsat imagery in forest disturbance mapping (Healey et al., 2005). However, we did not use the Tasseled Cap transformation in our analysis. Unlike Landsat TM and ETM+, Tasseled Cap coefficients have not been developed for MSS imagery that has been converted to reflectance data (Schowengerdt, 2007). Our normalization process depended on normalized reflectance values and not Digital Numbers. The established Tasseled Cap transformation can only be applied to Landsat MSS imagery in Digital Numbers.

We chose to classify the continuous output into three categories based on natural breaks in the data. Although relative differences are taken into account, the threshold between each class is somewhat subjective. Prior investigators have used lower thresholds (low <= 10%, moderate (11-29%), and severe > 30% of stands killed) (Aukema et al., 2006) or additional classes of mortality severity (e.g. trace, light, moderate, severe, and very severe) (Meddens et al., 2012). However, these two studies were considering ADS data which contained a measure of the number of trees or the percentage of stand killed. This type of classification scheme does not translate directly to our model. For example, if 15% of the trees were killed in a localized area, it could have a large impact on the reflectance of those pixels and overestimate the severity. This issue could be exacerbated by the coarse resolution of Landsat MSS pixels. Given that there is no precedent for this type of analysis we opted for a natural break classification scheme.

Our modeling framework was exhaustive in using multiple lines of evidence that represented the best available data. Our model incorporated the full extent of available spectral reflectance in MSS imagery (green, red and near infrared bands). Only band 3 was discarded given that it was highly correlated with band 4. Furthermore, the spectral information used by the model can be readily interpreted. NDVI is a commonly used index to assess ecological change (Pettorelli et al., 2005) and its behavior can be reasonably predicted from plant physiology theory (Garrity et al., 2013). Plant material containing chlorophyll reflects in the green wavelength. The reflectance in the green band would be expected to decrease as the amount of chlorophyll in a pixel is reduced from plant mortality. Therefore, the inclusion of the green band provides a measure of the amount of chlorophyll present within a pixel over time.

5. Conclusions

We have presented a framework that incorporates multiple lines of evidence to retrospectively characterize a landscape scale mountain pine beetle disturbance. Furthermore, we have demonstrated that Landsat MSS data is a valuable tool to extend the moderate resolution imagery record back to the early 1970s. We conclude that our approach is suitable to characterize the extent and severity of the event despite initial data limitations. Key considerations of the application of our model include the size and severity of the disturbance, as well as the timing (first date, last date, and duration) of the satellite imagery. Our approach captures the characteristics of a disturbance event that significantly impacts numerous ecological processes. Given the availability of these data sources, the characterization of recent events will afford investigators additional tools to study disturbance interactions and ecological legacies at the landscape scale.

Acknowledgements

This research was supported by an NPS grant through the Rocky Mountains Cooperative Ecosystem Studies Unit (IMR H1200090004), logistical support was provided by the USGS Fort Collins Science Center, and satellite imagery provided by the USGS Earth Resources Observation Systems Data Center. We thank Jeffrey Morisette for his comments that helped to improve the manuscript. We thank the following people for discussion on research direction and/or provision of data: Dennis Divoky, Sheree West, Jeff Hicke, Michael O'Donnell, Dan Manier, Alexandra Urza and Sayat Temirbekov.

References

Ahern, F. J. (1988). The effects of bark beetle stress on the foliar spectral reflectance of lodgepole pine. *International Journal of Remote Sensing*, *9*(9), 1451–1468.

Allen, C. D., & Breshears, D. D. (1998). Drought-induced shift of a forest-woodland ecotone: rapid landscape response to climate variation. *Proceedings of the National Academy of Sciences*, *95*(25), 14839–42.

Aukema, B. H., Carroll, A. L., Zhu, J., Raffa, K. F., Sickley, T. A., & Taylor, S. W. (2006). Landscape level analysis of mountain pine beetle in British Columbia, Canada: spatiotemporal development and spatial synchrony within the present outbreak. *Ecography*, *29*, 427–441.

Baker, W. L., Flaherty, P. H., Lindemann, J. D., Veblen, T. T., & Eisenhart, K. (2002). Effect of vegetation on the impact of a severe blowdown in the southern Rocky Mountains, USA. *Forest Ecology and Management*, *168*(1-3), 63–75. doi:10.1016/S0378-1127(01)00730-7

Bebi, P., Kulakowski, D., & Veblen, T. T. (2003). Interactions between Fire and Spruce Beetles in a Subalpine Rocky Mountain Forest Landscape. *Ecology*, *84*(2), 362–371.

Bentz, B. J., Régnière, J., Fettig, C. J., Hansen, E. M., Hayes, J. L., Hicke, J. A., Kelsey, R. G., Negrón, J. F., & Seybold, S. J. (2010). Climate Change and Bark Beetles of the Western United States and Canada: Direct and Indirect Effects. *BioScience*, *60*(8), 602–613. doi:10.1525/bio.2010.60.8.6

Bradley, B. A., & Fleishman, E. (2008). Relationships between expanding pinyon–juniper cover and topography in the central Great Basin, Nevada. *Journal of Biogeography*, *35*(5), 951–964. doi:10.1111/j.1365-2699.2007.01847.x

Brown, K., Hansen, A. J., Keane, R. E., & Graumlich, L. J. (2006). Complex interactions shaping aspen dynamics in the Greater Yellowstone Ecosystem. *Landscape Ecology*, *21*(6), 933–951. doi:10.1007/s10980-005-6190-3

Carreiras, J. M. B., Pereira, J. M. C., & Pereira, J. S. (2006). Estimation of tree canopy cover in evergreen oak woodlands using remote sensing. *Forest Ecology and Management*, *223*(1-3), 45–53. doi:10.1016/j.foreco.2005.10.056

Chander, G., Markham, B. L., & Helder, D. L. (2009). Remote Sensing of Environment Summary of current radiometric calibration coefficients for Landsat MSS , TM , ETM + , and EO-1 ALI sensors. *Remote Sensing of Environment*, *113*(5), 893–903. doi:10.1016/j.rse.2009.01.007

Chavez, P. S. (1988). An improved dark-object subtraction technique for atmospheric scattering correction of multispectral data. *Remote Sensing of Environment*, *24*(3), 459–479. doi:10.1016/0034-4257(88)90019-3

Chavez, P. S. (1996). Image-Based Atmospheric Corrections - Revisited and Improved. *Photogrammetric Engineering & Remote Sensing*, *62*(9), 1025–1036.

Cohen, W. B., Maiersperger, T. K., Spies, T. A., & Oetter, D. R. (2001). Modelling forest cover attributes as continuous variables in a regional context with Thematic Mapper data. *International Journal of Remote Sensing*, *22*(12), 2279–2310. doi:10.1080/01431160121472

Coops, N. C., Johnson, M., Wulder, M. A., & White, J. C. (2006). Assessment of QuickBird high spatial resolution imagery to detect red attack damage due to mountain pine beetle infestation. *Remote Sensing of Environment*, *103*(1), 67–80. doi:10.1016/j.rse.2006.03.012

Cressie, N. A. (1993). *Statistics for Spatial Data* (Revised., p. 928). New York, NY: Wiley-Interscience. doi:978-0471002550

Davidson, A., Aycrigg, J., Grossmann, E., Kagan, J., Lennartz, S., McDonough, S., Miewald, T., Ohmann, J., Radel, A., Sajwaj, T., & Tobalske, C. (2009). Digital Land Cover Map for the Northwestern United States. Moscow, ID: Northwest Gap Analysis Project: USGS GAP Analysis Program.

Dennison, P. E., Brunelle, A. R., & Carter, V. A. (2010). Assessing canopy mortality during a mountain pine beetle outbreak using GeoEye-1 high spatial resolution satellite data. *Remote Sensing of Environment*, *114*(11), 2431–2435. doi:10.1016/j.rse.2010.05.018

DeRose, R. J., Long, J. N., & Ramsey, R. D. (2011). Combining dendrochronological data and the disturbance index to assess Engelmann spruce mortality caused by a spruce beetle outbreak in southern Utah, USA. *Remote Sensing of Environment*, *115*(9), 2342–2349. doi:10.1016/j.rse.2011.04.034

Di Orio, A. P., Callas, R., & Schaefer, R. J. (2005). Forty-eight year decline and fragmentation of aspen (Populus tremuloides) in the South Warner Mountains of California. *Forest Ecology and Management*, *206*(1-3), 307–313. doi:10.1016/j.foreco.2004.11.011

Fettig, C. J., Klepzig, K. D., Billings, R. F., Munson, A. S., Nebeker, T. E., Negrón, J. F., & Nowak, J. T. (2007). The effectiveness of vegetation management practices for prevention and control of bark beetle infestations in coniferous forests of the western and southern United States. *Forest Ecology and Management*, *238*(1-3), 24–53. doi:10.1016/j.foreco.2006.10.011

Fuller, D. O. (2001). Forest fragmentation in Loudoun County , Virginia , USA evaluated with multitemporal Landsat imagery. *Landscape Ecology*, *16*, 627–642.

Garrity, S. R., Allen, C. D., Brumby, S. P., Gangodagamage, C., McDowell, N. G., & Cai, D. M. (2013). Quantifying tree mortality in a mixed species woodland using multitemporal high spatial resolution satellite imagery. *Remote Sensing of Environment*, *129*, 54–65. doi:10.1016/j.rse.2012.10.029

Gitelson, A. A., Kaufman, Y. J., & Merzlyak, M. N. (1996). Use of a Green Channel in Remote Sensing of Global Vegetation from EOS-MODIS. *Remote Sensing of Environment*, *58*(3), 289–298.

Goodwin, N. R., Coops, N. C., Wulder, M. A., Gillanders, S., Schroeder, T. A., & Nelson, T. (2008). Estimation of insect infestation dynamics using a temporal sequence of Landsat data. *Remote Sensing of Environment*, *112*, 3680–3689. doi:10.1016/j.rse.2008.05.005

Goodwin, N. R., Magnussen, S., Coops, N. C., & Wulder, M. A. (2010). Curve fitting of time-series Landsat imagery for characterizing a mountain pine beetle infestation. *International Journal of Remote Sensing*, *31*(12), 3263–3271. doi:10.1080/01431160903186277

Hamel, D., McGregor, M., & Oakes, R. (1977). Status of Mountain Pine Beetle Infestation Glacier National Park, 1976. Missoula, MT.

Harris, J., Dawson, A. F., & Goodenough, D. (1978). Evaluation of LANDSAT Data for Forest Pest Detection and Damage Appraisal Surveys in British Columbia. *Report BC-X-182*. Victoria, BC: Pacific Forest Research Centre.

Healey, S., Cohen, W., Zhiqiang, Y., & Krankina, O. (2005). Comparison of Tasseled Cap-based Landsat data structures for use in forest disturbance detection. *Remote Sensing of Environment*, *97*(3), 301–310. doi:10.1016/j.rse.2005.05.009

Hevesi, J. A., Istok, J. D., & Flint, A. L. (1992). Precipitation Estimation in Mountainous Terrain Using Multivariate Geostatistics. Part I: Structural Analysis. *Journal of Applied Meteorology*, *31*, 661–676.

Hicke, J., & Logan, J. (2009). Mapping whitebark pine mortality caused by a mountain pine beetle outbreak with high spatial resolution satellite imagery. *International Journal of Remote Sensing*, *30*(17), 4427–4441. doi:10.1080/01431160802566439

Homer, C., Dewitz, J., Fry, J., Coan, M., Hossain, N., Larson, C., Herold, N., Mckerrow, A., Vandriel, J. N., & Wickham, J. (2007). Completion of the 2001 National Land Cover Database for the Conterminous United States. *Photogrammetric Engineering & Remote Sensing*, 337–341.

Homer, C., Huang, C., Yang, L., Wylie, B., & Coan, M. (2004). Development of a 2001 National Land-Cover Database for the United States. *Photogrammetric Engineering & Remote Sensing*, *70*(7), 829–840.

Huang, C., Asner, G. P., Barger, N. N., Neff, J. C., & Floyd, M. L. (2010). Regional aboveground live carbon losses due to drought-induced tree dieback in piñon–juniper ecosystems. *Remote Sensing of Environment*, *114*(7), 1471–1479. doi:10.1016/j.rse.2010.02.003

Johnson, E. A., & Fryer, G. I. (1987). Historical vegetation change in the Kananaskis Valley, Canadian Rockies. *Canadian Journal of Botany*, *65*(5), 853–858. doi:10.1139/b87-116

Jones, H. G., & Vaughan, R. H. (2010). *Remote Sensing of Vegetation: Principles, Techniques, and Applications* (p. 400). Oxford, UK: Oxford University Press.

Kadmon, R., & Harari-Kremer, R. (1999). Studying Long-Term Vegetation Dynamics Using Digital Processing of Historical Aerial Photographs. *Remote Sensing of Environment*, *68*(2), 164–176. doi:10.1016/S0034-4257(98)00109-6

Kennedy, R., & Spies, T. (2004). Forest cover changes in the Oregon Coast Range from 1939 to 1993. *Forest Ecology and Management*, *200*, 129–147. doi:10.1016/j.foreco.2003.12.022

Lefsky, M., & Cohen, W. (2003). Selection of remotely sensed data. In M. A. Wulder & S. Franklin (Eds.), *Remote Sensing of Forest Environments: Concepts and Case Studies* (pp. 13–47). Boston: Kluwer Academic Publishers.

Legendre, P., & Fortin, M. (1989). Spatial Pattern and Ecological Analysis. *Vegetatio*, *80*(2), 107–138.

Logan, J. A., & Powell, J. A. (2001). Ghost Forests, Global Warming, and the Mountain Pine Beetle (Coleoptera: Scolytidae). *American Entomologist*, *47*(3), 160–173.

Manier, D. J., Hobbs, N. T., Theobald, D. M., Reich, R. M., Kalkhan, M. A., & Campbell, M. R. (2005). Canopy dynamics and human caused disturbance on a semi-arid landscape in the Rocky Mountains, USA. *Landscape Ecology*, *20*(1), 1–17. doi:10.1007/s10980-004-3987-4

Maselli, F. (2004). Monitoring forest conditions in a protected Mediterranean coastal area by the analysis of multiyear NDVI data. *Remote Sensing of Environment*, *89*(4), 423–433. doi:10.1016/j.rse.2003.10.020

Mauseth, J. (1988). *Plant Anatomy* (First Ed., p. 560). Menlo Park, CA: The Benjamin/Cummings Publishing Company.

McGregor, M., Hamel, D., Lood, R., & Meyer, H. (1975). Status of Mountain Pine Beetle Infestation Glacier National Park, 1974. Missoula, MT.

Meddens, A. J. H., Hicke, J. A., & Ferguson, C. A. (2012). Spatiotemporal patterns of observed bark beetle-caused tree mortality in British Columbia and the western United States. *Ecological Applications*, *22*(7), 1876–1891.

Meddens, A. J. H., Hicke, J. A., & Vierling, L. A. (2011). Evaluating the potential of multispectral imagery to map multiple stages of tree mortality. *Remote Sensing of Environment*, *115*(7), 1632–1642. doi:10.1016/j.rse.2011.02.018

Meddens, A. J. H., Hicke, J. A., Vierling, L. A., & Hudak, A. T. (2013). Evaluating methods to detect bark beetle-caused tree mortality using single-date and multi-date Landsat imagery. *Remote Sensing of Environment*, *132*, 49–58. doi:10.1016/j.rse.2013.01.002

Meigs, G. W., Kennedy, R. E., & Cohen, W. B. (2011). A Landsat time series approach to characterize bark beetle and defoliator impacts on tree mortality and surface fuels in conifer forests. *Remote Sensing of Environment*, *115*(12), 3707–3718. doi:10.1016/j.rse.2011.09.009

Millar, C. I., Stephenson, N. L., & Stephens, S. L. (2007). Climate change and forests of the future: managing in the face of uncertainty. *Ecological Applications*, *17*(8), 2145–51.

Moran, M. S., Jackson, R. D., Slater, P. N., & Teiuet, P. M. (1992). Evaluation of Simplified Procedures for Retrieval of Land Surface Reflectance Factors from Satellite Sensor Output. *Remote Sensing of Environment*, *41*, 169–184.

NASA. (2013). The Multispectral Scanner System. Retrieved April 15, 2013, from http://landsat.gsfc.nasa.gov/about/mss.html

Nemani, R., Hashimoto, H., Votava, P., Melton, F., Wang, W., Michaelis, A., Mutch, L., Milesi, C., Hiatt, S., & White, M. (2009). Monitoring and forecasting ecosystem dynamics using the Terrestrial Observation and Prediction System (TOPS). *Remote Sensing of Environment*, *113*(7), 1497–1509. doi:10.1016/j.rse.2008.06.017

Parmenter, A. W., Hansen, A. J., Kennedy, R. E., Cohen, W. B., Langner, U., Lawrence, R., Maxwell, B., Gallant, A., & Aspinall, R. (2003). Land Use and Land Cover Change in the Greater Yellowstone Ecosystem: 1975 – 1995. *Ecological Applications*, *13*(3), 687–703.

Pettorelli, N., Vik, J. O., Mysterud, A., Gaillard, J. M., Tucker, C. J., & Stenseth, N. C. (2005). Using the satellite-derived NDVI to assess ecological responses to environmental change. *Trends in ecology & evolution*, *20*(9), 503–10. doi:10.1016/j.tree.2005.05.011

Platt, R. V., & Schoennagel, T. (2009). An object-oriented approach to assessing changes in tree cover in the Colorado Front Range 1938–1999. *Forest Ecology and Management*, *258*(7), 1342–1349. doi:10.1016/j.foreco.2009.06.039

Powell, J. A., & Logan, J. A. (2005). Insect seasonality: circle map analysis of temperature-driven life cycles. *Theoretical population biology*, *67*(3), 161–79. doi:10.1016/j.tpb.2004.10.001

R Development Core Team. (2011). R: A language and environment for statistical computing. Vienna, Austria: R Foundation for Statistical Computing. Retrieved from http://www.r-project.org/

Raffa, K. F., Aukema, B. H., Bentz, B. J., Carroll, A. L., Hicke, J. A., Turner, M. G., & Romme, W. H. (2008). Cross-scale Drivers of Natural Disturbances Prone to Anthropogenic

Amplification: The Dynamics of Bark Beetle Eruptions. *BioScience*, *58*(6), 501. doi:10.1641/B580607

Reich, R. M., Aguirre-Bravo, C., Bravo, V. A., & Briseño, M. M. (2011). Empirical evaluation of confidence and prediction intervals for spatial models of forest structure in Jalisco, Mexico. *Journal of Forestry Research*, *22*(2), 159–166. doi:10.1007/s11676-011-0144-1

Rencz, A. N., & Nemeth, J. (1985). Detection of Mountain Pine Beetle Infestation Using Landsat MSS and Simulated Thematic Mapper Data. *Canadian Journal of Remote Sensing*, *11*(1), 50–58.

Rousse, J. W., Hass, R. H., Schell, J. A., Deering, D. W., & Harlan, J. C. (1974). Monitoring the vernal advancement of retrogradation of natural vegetation. *Type III, Final Report*. Greenbelt, Maryland.

Schott, J. R., Salvaggio, C., & Volchok, W. J. (1988). Radiometric Scene Normalization Using Pseudoinvariant Features. *Remote Sensing of Environment*, *26*, 1–16.

Schowengerdt, R. A. (2007). *Remote Sensing: Models and Methods for Image Processing* (Third Ed., p. 560). San Diego: Academic Press, San Diego, CA.

Schroeder, T. A., Cohen, W. B., Song, C., Canty, M. J., & Yang, Z. (2006). Radiometric correction of multi-temporal Landsat data for characterization of early successional forest patterns in western Oregon. *Remote Sensing of Environment*, *103*, 16 – 26. doi:10.1016/j.rse.2006.03.008

Skakun, R. S., Wulder, M. A., & Franklin, S. E. (2003). Sensitivity of the thematic mapper enhanced wetness difference index to detect mountain pine beetle red-attack damage. *Remote Sensing of Environment*, *86*(4), 433–443. doi:10.1016/S0034-4257(03)00112-3

Strand, E., Smith, A., Bunting, S., Vierling, L., Hann, D., & Gessler, P. (2006). Wavelet estimation of plant spatial patterns in multitemporal aerial photography. *International Journal of Remote Sensing*, *27*(10), 2049–2054. doi:10.1080/01431160500444764

Swetnam, T. W., Allen, C. D., & Betancourt, J. L. (1999). Applied Historical Ecology: Using the Past To Manage for the Future. *Ecological Applications*, *9*(4), 1189–1206. doi:10.1890/1051-0761(1999)009[1189:AHEUTP]2.0.CO;2

Townsend, P. A., Singh, A., Foster, J. R., Rehberg, N. J., Kingdon, C. C., Eshleman, K. N., & Seagle, S. W. (2012). A general Landsat model to predict canopy defoliation in broadleaf deciduous forests. *Remote Sensing of Environment*, *119*, 255–265. doi:10.1016/j.rse.2011.12.023

Townshend, J. R., Masek, J. G., Huang, C., Vermote, E. H., Gao, F., Channan, S., Sexton, J. O., Feng, M., Narasimhan, R., Kim, D., Song, K., Song, D., Song, X., Noojipady, P., Tan, B., Hansen, M. C., Li, M., & Wolfe, R. E. (2012). Global characterization and monitoring of forest cover using Landsat data: opportunities and challenges. *International Journal of Digital Earth*, *5*(5), 373–397.

Turner, M. G., & Dale, V. H. (1998). Comparing Large, Infrequent Disturbances: What Have We Learned? *Ecosystems*, *1*, 493–496.

Turner, M. G., Hargrove, W. W., Gardner, R. H., & Romme, W. H. (1994). Effects of Fire on Landscape Heterogeneity in Yellowstone National Park, Wyoming. *Journal of Vegetation Science*, *5*, 731–742.

Upton, G. J. G., & Fingleton, B. (1985). *Spatial data Analysis by Example. Volume 1: Point Pattern and Quantitative Data* (p. 410). Chichester: John Wiley & Sons.

USGS. (2012). EarthExplorer archive. Retrieved March 01, 2012, from http://edcsns17.cr.usgs.gov/NewEarthExplorer/

Veblen, T. T., Hadley, K. S., Nel, E. M., Kitzberger, T., Reid, M., & Villalba, R. (1994). Disturbance regime and disturbance interactions in a Rocky Mountain subalpine forest. *Journal of Ecology*, *82*, 125–135.

Vicente-Serrano, S., Perezcabello, F., & Lasanta, T. (2008). Assessment of radiometric correction techniques in analyzing vegetation variability and change using time series of Landsat images. *Remote Sensing of Environment*, *112*(10), 3916–3934. doi:10.1016/j.rse.2008.06.011

Vogelmann, J. E., Tolk, B., & Zhu, Z. (2009). Monitoring forest changes in the southwestern United States using multitemporal Landsat data. *Remote Sensing of Environment*, *113*(8), 1739–1748. doi:10.1016/j.rse.2009.04.014

Vogelmann, J. E., Xian, G., Homer, C., & Tolk, B. (2012). Monitoring gradual ecosystem change using Landsat time series analyses: Case studies in selected forest and rangeland ecosystems. *Remote Sensing of Environment*, *122*, 92–105. doi:10.1016/j.rse.2011.06.027

Volcani, A., Karnieli, A., & Svoray, T. (2005). The use of remote sensing and GIS for spatio-temporal analysis of the physiological state of a semi-arid forest with respect to drought years. *Forest Ecology and Management*, *215*(1-3), 239–250. doi:10.1016/j.foreco.2005.05.063

Weber, F. P., Roberts, E. H., & Waite, T. H. (1975). Forest Stress Detection: Ponderosa Pine Mortality from Mountain Pine Beetle. In *Evaluation of ERTS-1 Data for Forest and Rangeland Surveys* (pp. 44–61). Berkeley, California: USDA Forest Service Research Paper PSW-112.

White, J., Wulder, M. A., Brooks, D., Reich, R., & Wheate, R. (2005). Detection of red attack stage mountain pine beetle infestation with high spatial resolution satellite imagery. *Remote Sensing of Environment*, *96*(3-4), 340–351. doi:10.1016/j.rse.2005.03.007

Woodcock, C., Allen, R., Anderson, M., Belward, A., Bindschadler, R., Cohen, W., Gao, F., Goward, S., Helder, D., Helmer, E., Nemani, R., Oreopoulos, L., Schott, J., Thenkabail, P., Vermote, E., Vogelmann, J., Wulder, M. A., & Wynne, R. (2008). Free Access to Landsat Imagery. *Science*, *320*, 1011.

Wulder, M. A., Dymond, C., White, J. C., Leckie, D. G., & Carroll, A. L. (2006a). Surveying mountain pine beetle damage of forests: A review of remote sensing opportunities. *Forest Ecology and Management*, *221*, 27–41.

Wulder, M. A., White, J. C., Bentz, B. J., Alvarez, M. F., & Coops, N. C. (2006b). Estimating the probability of mountain pine beetle red-attack damage. *Remote Sensing of Environment*, *101*, 150–166.

Yuan, D., & Elvidge, C. D. (1996). Comparison of relative radiometric normalization techniques. *Photogrammetry and Remote Sensing*, *51*(3), 117–126. doi:10.1016/0924-2716(96)00018-4

Table 1. Spectral characteristics of Landsat MSS imagery (NASA, 2013).

Band	Wavelength	Spectral Region
1	500-600 nm	Green
2	600-700 nm	Red
3	700-800 nm	Near-infrared
4	800-1100 nm	Near-infrared

Table 2. Satellite imagery scene information and acquisition date used in the analysis.

Satellite	Scene Path/Row	Acquisition Date (year-month-day)
Landsat 1	44/26	19730910
Landsat 1	44/26	19740923
Landsat 2	44/26	19760921
Landsat 2	44/26	19770811
Landsat 3	44/26	19780902
Landsat 3	44/26	19790915
Landsat 2	44/26	19810913
Landsat 4	41/26	19830924
Landsat 5	41/26	19870911

Table 3. Spectral indices calculated with the Landsat MSS reflectance data; NDVI (Normalized Difference Vegetation Index), RGI (Red Green Index), and GNDVI (Green Normalized Difference Vegetation Index).

Spectral Index	Equation	Source
NDVI	$NDVI = MSS_{Band4} – MSS_{Band2}/MSS_{Band4} + MSS_{Band2}$	Rousse et al. 1974
RGI	$RGI = MSS_{Band2}/MSS_{Band1}$	Coops et al. 2006
GNDVI	$GNDVI = MSS_{Band4} – MSS_{Band1}/MSS_{Band4} + MSS_{Band1}$	Gitelson et al. 1996

Table 4. Descriptive statistics of estimated tree canopy mortality from the aerial photo plots grouped by aspect class (*n*=267).

Aspect	**Number of Plots**	**Tree Canopy Mortality Statistics**			
		Mean	**Minimum**	**Maximum**	**S.D.**
North	46	54.9	4.4	91.8	23.6
East	47	49.4	12.8	93.9	24.0
South	75	54.1	17.0	99.2	20.8
West	93	68.3	12.7	99.8	21.3

Table 5. Comparison of model evaluation metrics.

Model	**AIC**	**R^2**	**MAE**	**RMSE**	**10-fold Cross Validation Prediction Error**
NDVI + G	-237.55	0.65	10.8%	13.6%	15.4%
NDVI	-204.44	0.60	11.6%	14.5%	16.8%
PCA	-193.43	0.60	11.9%	14.6%	20.4%
GNDVI	-183.13	0.55	12.4%	15.6%	17.3%
RGI	-87.32	0.34	15.3%	18.8%	20.7%

Table 6. Predictor variables used in the NDVI + G GLS model. Estimates of the model parameters are listed for the west and east sides accordingly. The variables *Aspect* and *Total # of Years* (low was the only category retained in the stepwise model) were treated as indicator variables in the analysis. **P-value* is significant at 0.05 or lower.

Variable	**West Coefficient**	**East Coefficient**
(Intercept)	3.18413*	3.43654*
Aspect		
N	0.13478	-1.42706*
S	-0.24309	-
W	-0.58963*	-0.17668*
green.1973	-9.58080*	-
green.1974	-8.60109*	-
green.1977	-9.97942*	-
green.1978	-10.69192*	-12.20042
green.1979	-5.24848	-
green.1983	6.49274	-
green.1987	8.11468*	-11.77014*
Total # of Years - Low	0.15773*	-
ndvi.1973	-	-0.37092
ndvi.1974	-0.03773	-
ndvi.1976	0.41517*	-
ndvi.1977	-1.08326*	-1.74362*
ndvi.1978	-0.36746	-
ndvi.1979	0.40112	-
ndvi.1981	-1.42992*	-
ndvi.1983	-0.40449*	-0.50511
ndvi.1973 x N	-	2.01483
ndvi.1974 x N	-1.24923*	-
ndvi.1978 x N	1.69811*	-
ndvi.1978 x W	1.10049*	-
ndvi.1979 x N	-1.78641*	-
ndvi.1979 x S	-1.18434*	-
ndvi.1979 x W	-1.49155*	-
ndvi.1981 x S	1.52377*	-
ndvi.1981 x W	1.20919*	-
ndvi.1983 x N	0.9887*	-

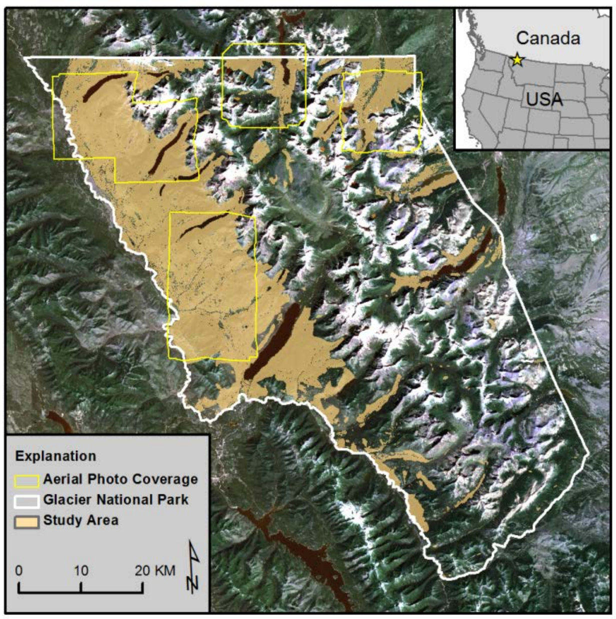

Figure 1. Location of study area and extent of aerial photo coverage. Background image is Landsat Thematic Mapper (TM) Imagery (bands 3, 2, 1) acquired on August 25, 2010. Yellow polygons represent the location and extent of aerial photograph coverage; tan area represents the confined study area.

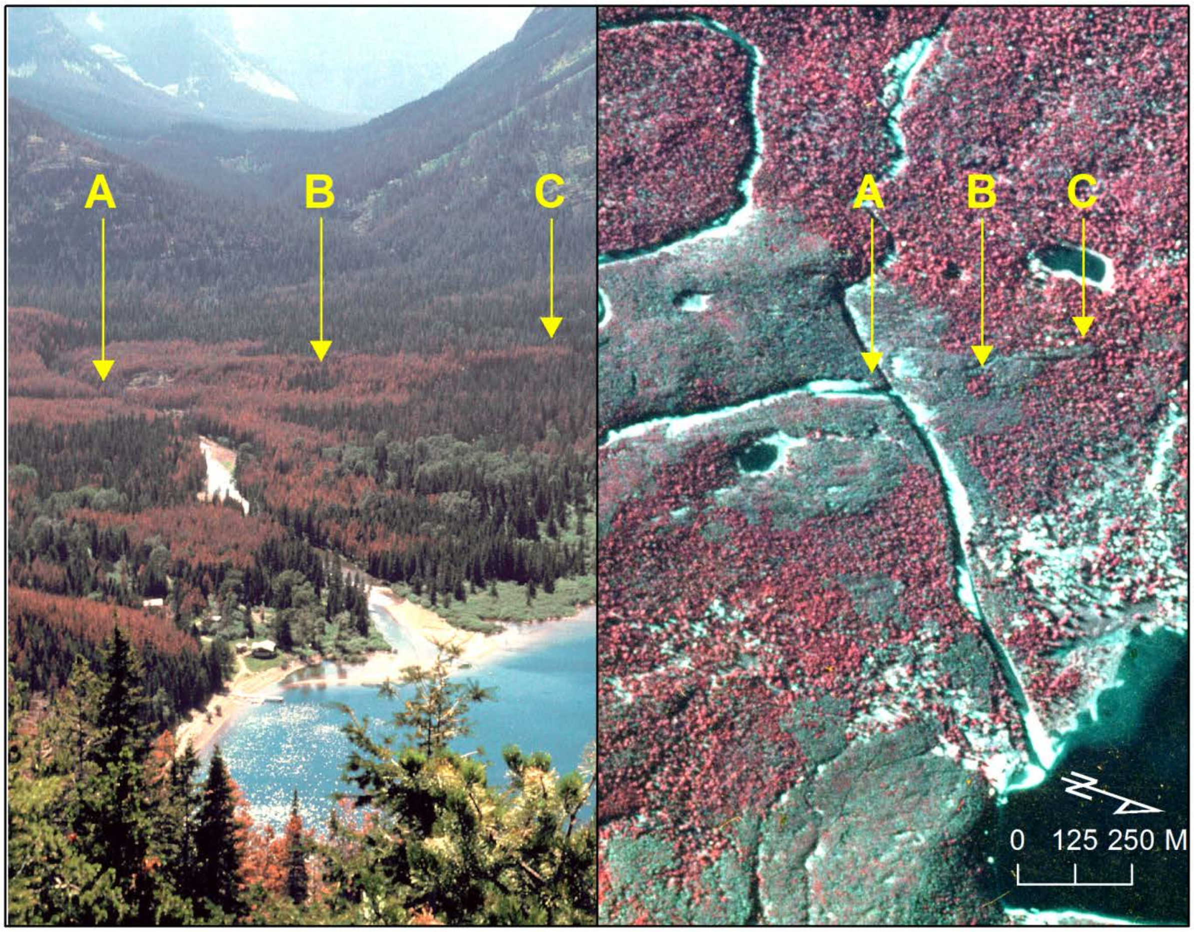

Figure 2. (Left) Landscape photo taken in the Summer of 1980 showing a mixture of live and dead trees in the red attack stage in Waterton Valley (source: Glacier National Park Research Library). (Right) A color-infrared aerial photo of the same area acquired in October 1980 (source: NASA/Glacier National Park). The mosaic of live and dead forest can be identified in both images. The letters correspond to the same area in each photo (A = stream confluence, B = small patch of live trees, surrounded by dead forest, C = linear ribbon of dead forest).

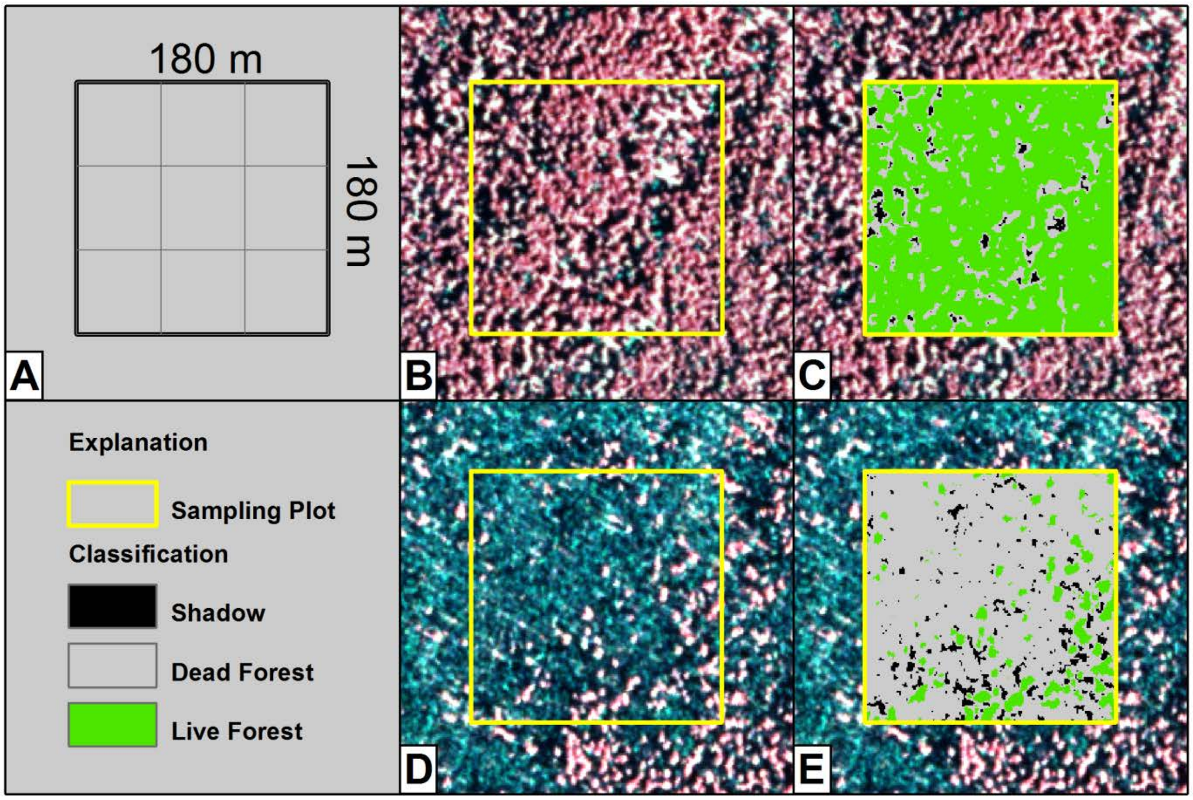

Figure 3. (A) Plot used to sample aerial photos. The 180 m x 180 m plot size was chosen to include a 3 x 3 block of Landsat MSS pixels. (B) Sampling plot overlaid on color infrared photo at a low mortality site. (D) Sampling plot overlaid on color infrared photo at a high mortality site. (C) Output classification from sampling plot in panel B (live canopy cover = 83%). (E) Output classification from sampling plot in panel D (live canopy cover = 10%).

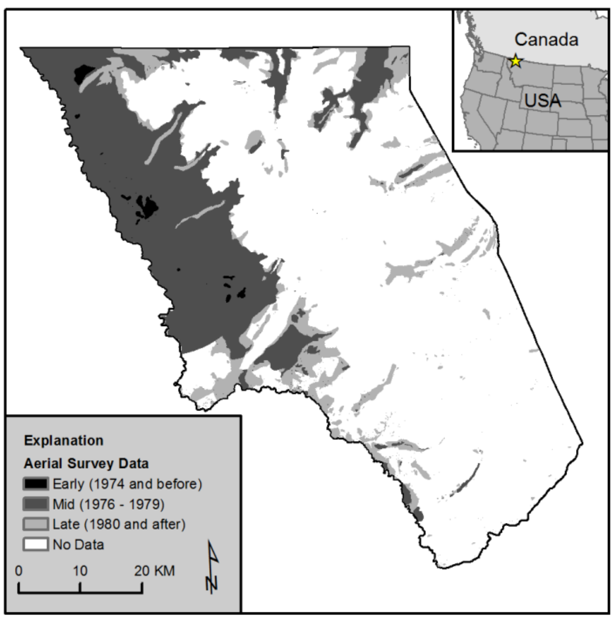

Figure 4. Mapped area impacted by mountain pine beetle according to the aerial detection survey data. Note: there was no data available for 1975.

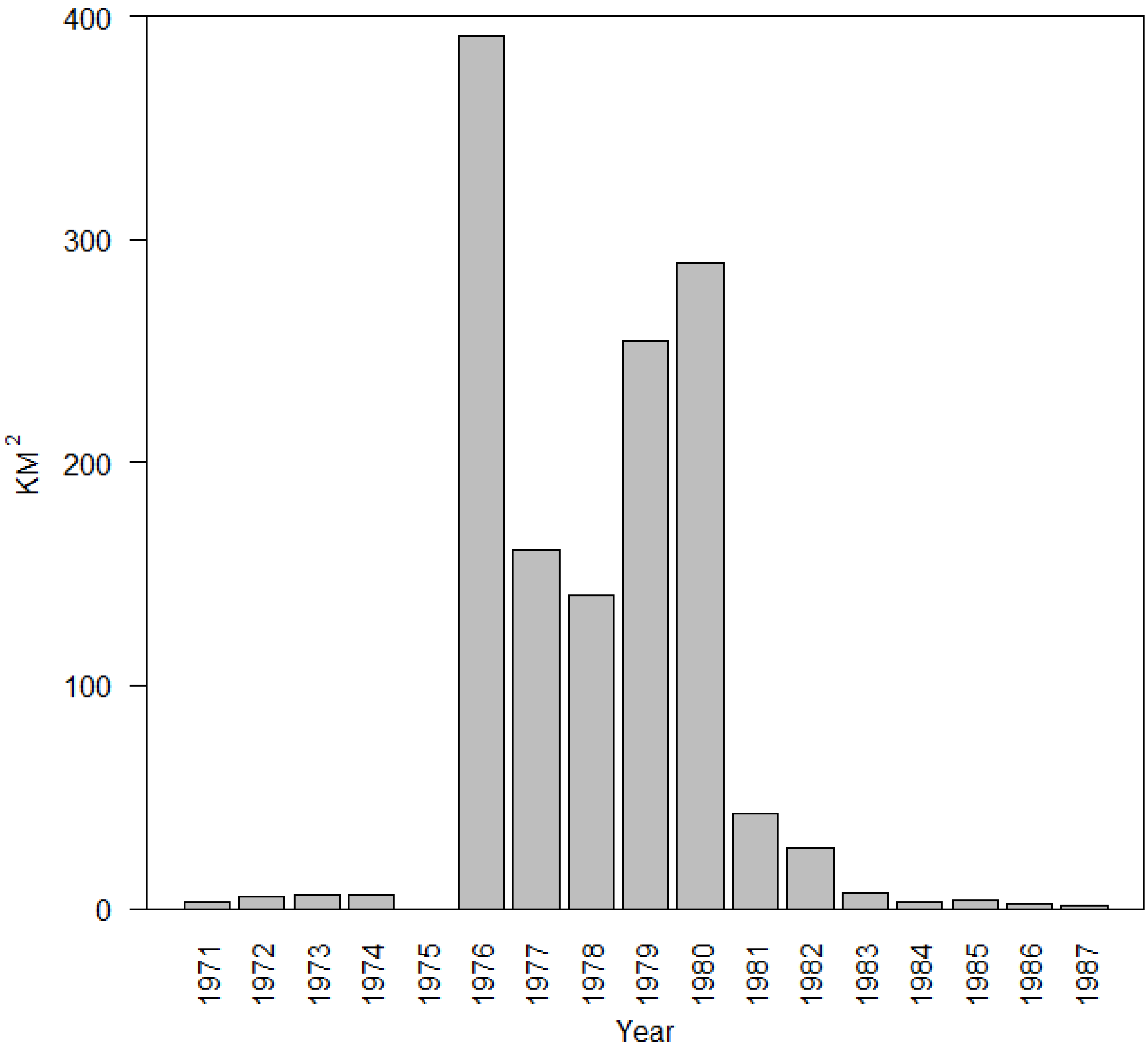

Figure 5. Area impacted by mountain pine beetle annually based on aerial detection survey data. Note: there was no data available for 1975.

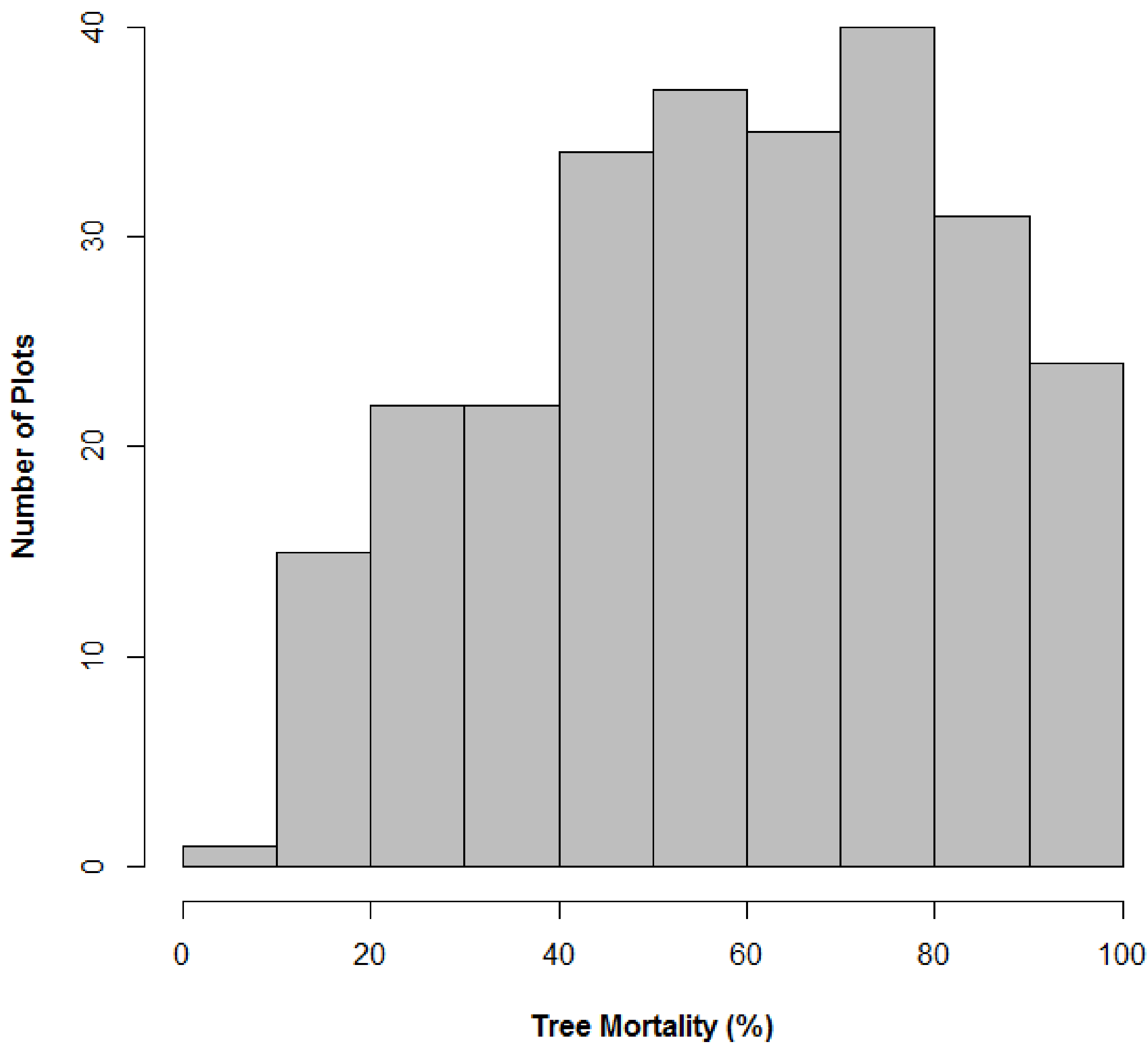

Figure 6. Histogram of canopy tree mortality (%) for all plots (*n*=267).

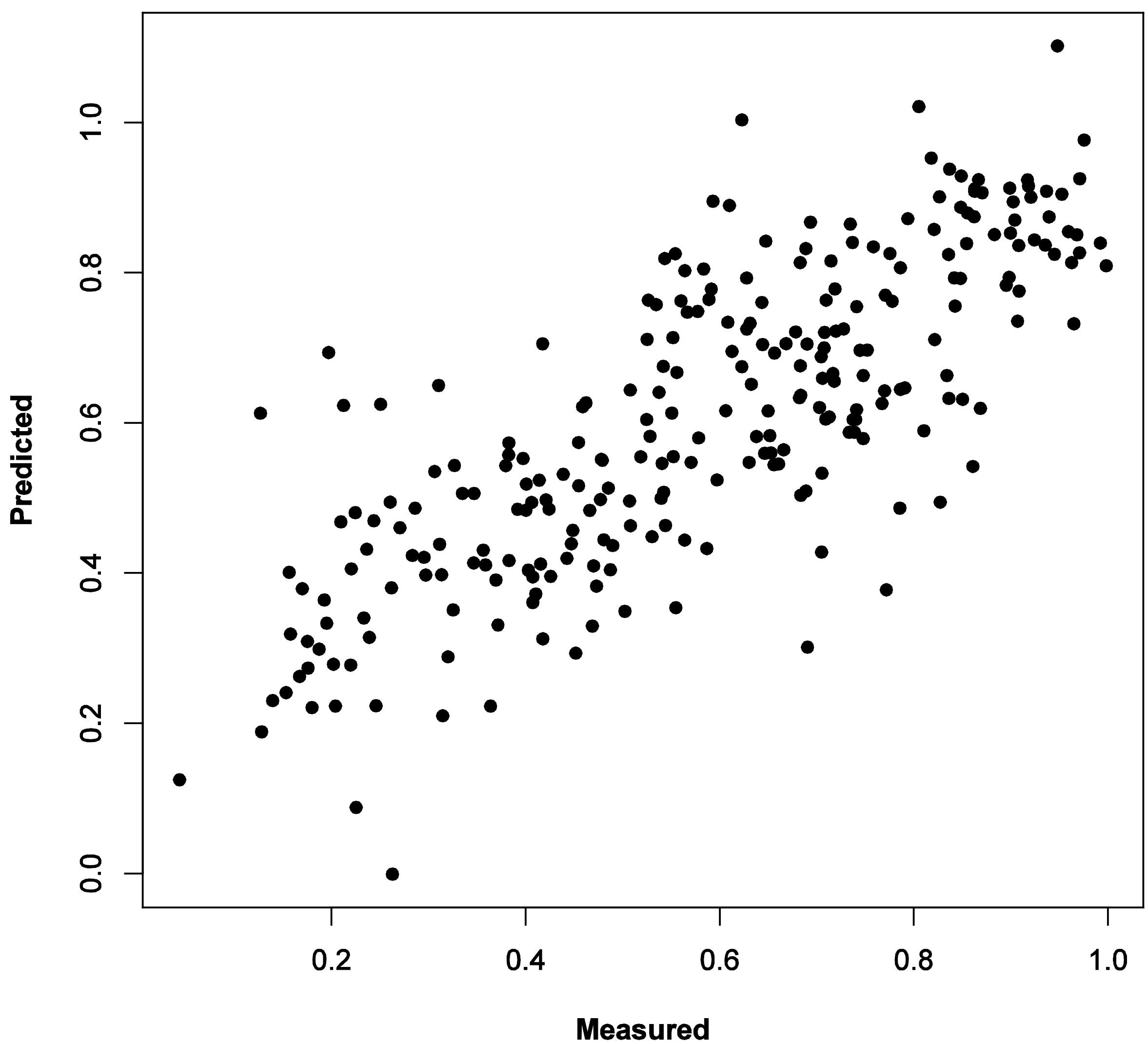

Figure 7. The output of the NDVI+G GLS model used to estimate canopy change over time due to mortality.

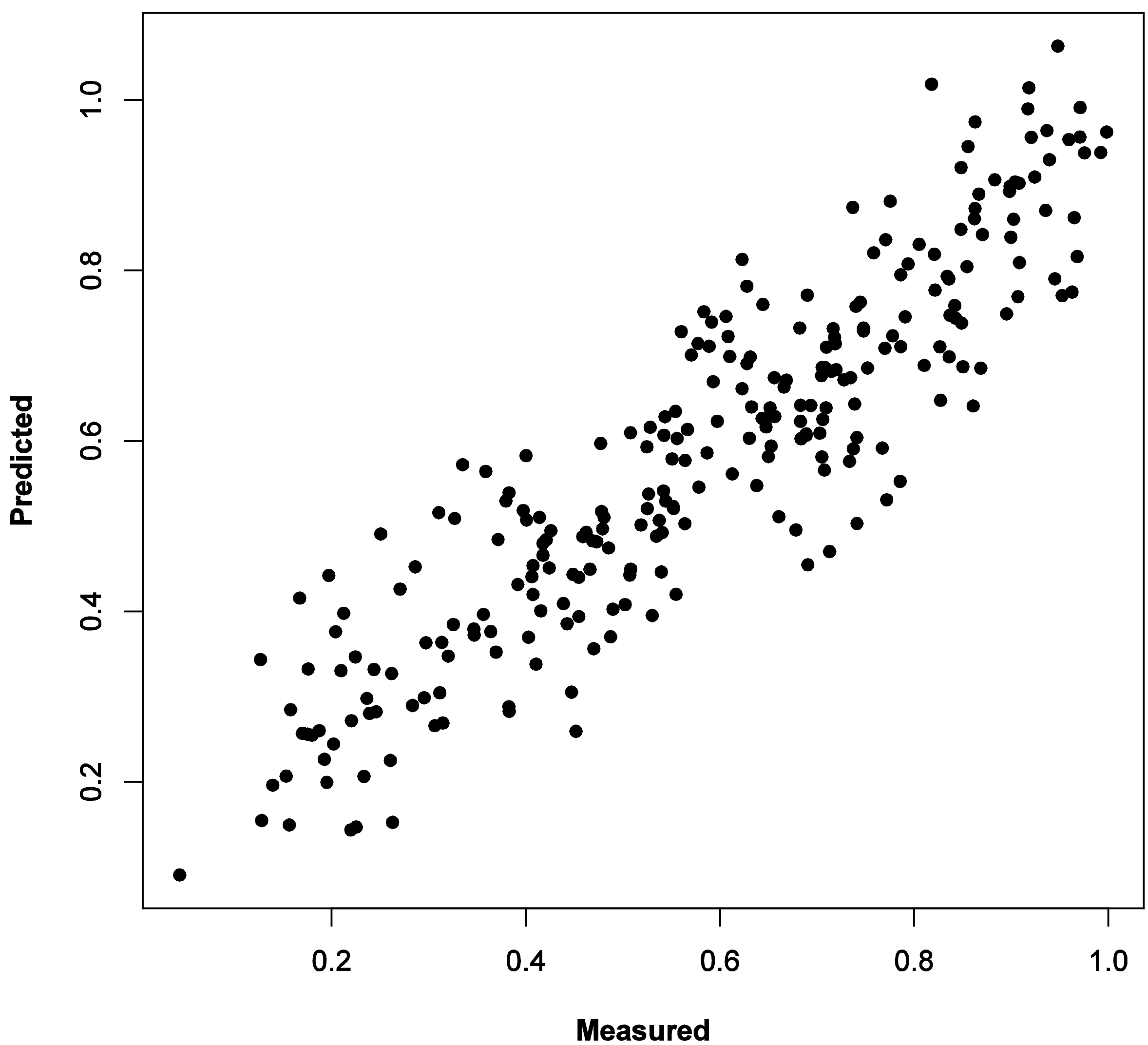

Figure 8. The output of the combined GLS-CART model used to estimate canopy change over time due to mortality.

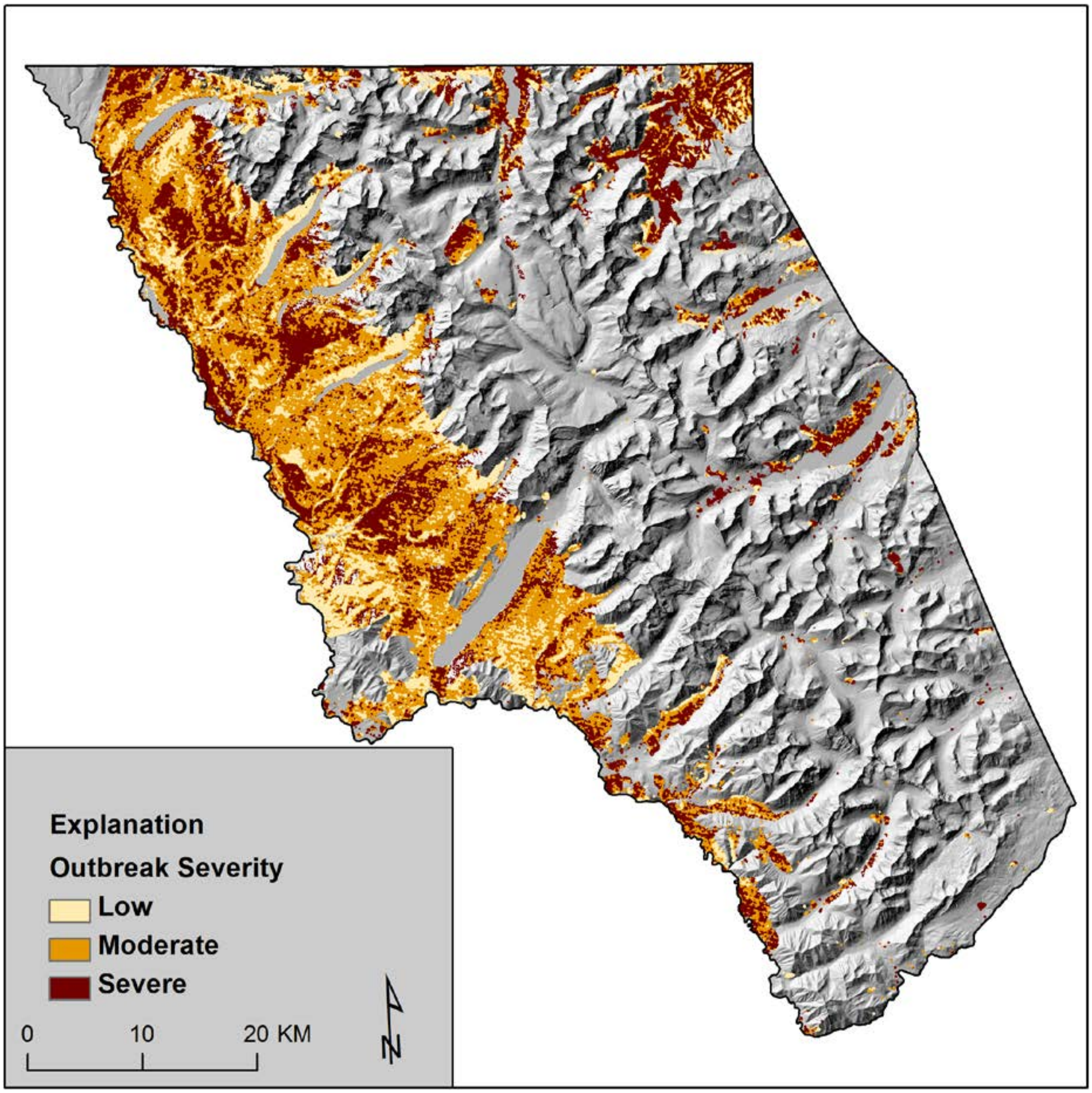

1014

1015 Figure 9. The output of the spatial model classified into three severity levels.

1016

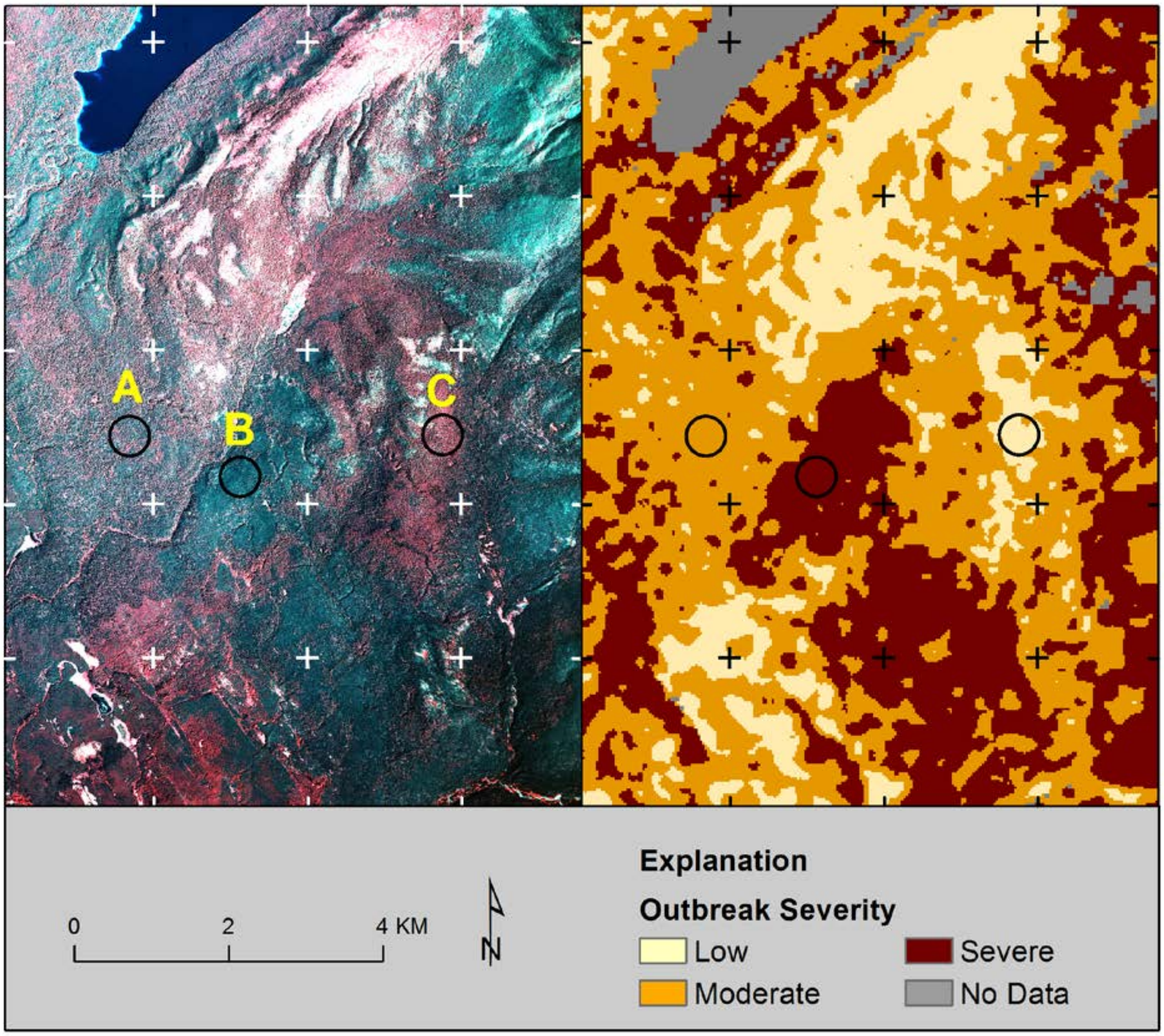

Figure 10. (Left) Color-infrared photo (year acquired = 1982). (Right) Classified map result of the same area (focal window applied). Black polygons correspond to spectral trajectories in Figure 11 (A=Moderate, B=Severe, C=Low). Note: tick marks are spaced on a 2 km grid; black polygons are 0.2 km^2 (20 hectares) in size.

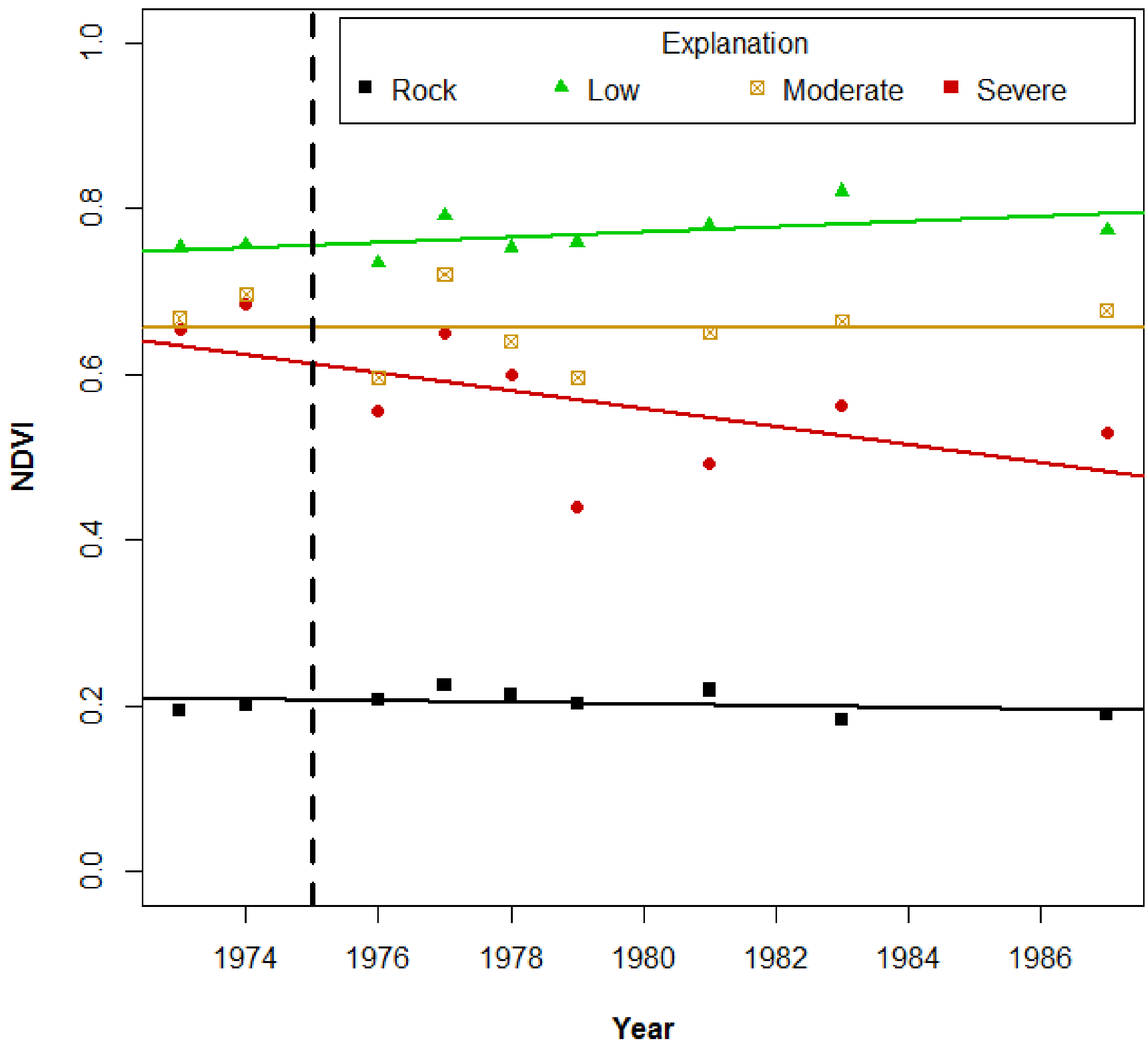

Figure 11. Spectral trajectories of classified outbreak severity. The three trajectories correspond to the polygons identified in Figure 10. Note: rock features are included to demonstrate the success of the image normalization process and the stability of pseudo-invariant features over time.